multiple gene fusion and fission events have occurred in various eukaryotic groups and this information sheds new light on the evolutionary concept of gene fusion. Crystals of dihydroorotate dehydrogenase, a *pyr4* gene product, were obtained by Inaoka *et al.* and provide important information for structure-based drug design [56]. Hashimoto *et al.* [57,58] reported that *T. cruzi* post-transcriptionally upregulates and exploits host c-FLIP for inhibition of a death-inducing signal. This mechanism enables the parasite to survive and results in Chagas disease. Kita and his group discovered ascofuranone, a novel inhibitor of parasite mitochondrial function. This compound blocks the cyanide-insensitive terminal oxidase of *Trypanosoma brucei brucei* mitochondria, an enzyme also known as trypanosome alternative oxidase [59]. In addition, this compound inhibits trypanosomal growth in heavily-infected mice and is a good lead for the development of new treatments for African trypanosomiasis [60]. The direct evidence that the motif $E(X)_6Y$ is essential for the activity of alternative oxidases (AOXs) was reported by Nakamura *et al.* [61]. AOXs have been found in *Cryptosporidium parvum* in addition to trypanosomes [62].

Nozaki and his group have been working to discover and exploit rational targets for the development of chemotherapeutics against *Entamoeba histolytica* infection. *E. histolytica* possesses unique metabolisms of sulfur-containing amino acids [63], particularly in sulfur-assimilatory *de novo* cysteine biosynthesis and degradation of methionine, homocysteine and cysteine. Methionine γ-lyase, which is the sole enzyme responsible for the degradation of cysteine, is a target for further drug development. Nozaki also showed unique aspects in vesicular trafficking that are involved in phagocytosis and intracellular transport of virulence factors, including cysteine proteases in *E. histolytica* [64–69]. The diversity of Rab small GTPases and isoprenylation enzymes of Ras, Rho/Rac and Rab small GTPases involved in the related processes seem to represent divergent and rational targets [70]. In particular, both farnesyltransferase and geranylgeranyltransferase I of *E. histolytica* were proven to be biochemically divergent in their sensitivity to known inhibitors.

Concluding remarks

Essential parasite-specific systems that differ from those of the host represent attractive targets for specialized chemotherapy, as illustrated by glutamate-gated chloride channels and the specific activator avermectin. Many people in developing countries still suffer or die from malaria, schistosomiasis, filariasis and other infectious diseases, whereas, in developed countries, parasitic infectious diseases, especially those that are caused by opportunistic infection resulting from immunosuppressants and HIV/AIDS, are increasing. Moreover, the emergence of strains that are resistant to the current front-line drugs is exacerbating an increasingly dire situation. Therefore, through the knowledge and understanding gained from basic research into parasites and the development of this research for clinical application, Japanese scientists have an important role at the forefront of the control of emerging and re-emerging parasitic diseases.

References

1 Ehrlich, P. and Shiga, K. (1904) Farbentherapeutische versuche bei Trypanosomenerkrankung. *Berlin Klin. Wochenschrift* 41, pp. 329–332 and pp. 362–365
2 Kagei, N. and Hayashi, S. (1999) Control of parasitoses in Japan. In *Progress of Medical Parasitology in Japan* (Vol. 7, Japanese edn) (Otsuru, M. *et al.*, eds), pp. 647–668, Meguro Parasitological Museum
3 Ichimori, K. *et al.* Lymphatic filariasis elimination in the Pacific: PacELF replicating Japanese success, *Trends Parasitol.* 23, 36–40
4 Nishi, M. (1922) Experimental treatment for Schistosomiasis japonica by tartar emetic. *J. Jpn. Soc. Int. Med.* 10, 143–145
5 Felter, H.W. and Lloyd, J.U., eds (1898) *King's American Dispensatory* (18th edn), Ohio Valley Co.
6 Suzuka, O. (1987) The domestic production of santonin at Kyoto – a review on H. Ichinose's works. *J. Jpn. His. Pharm.* 22, 7–10
7 Yokogawa, M. *et al.* (1963) Chemotherapy of paragonimiasis with bithionol v. studies on the minimum effective dose and changes in abnormal X-ray shadows in the chest after treatment. *Am. J. Trop. Med. Hyg.* 12, 859–869
8 Murakami, S. *et al.* (1953) Effective principle of *Digenea. Jpn. J. Pharm. Chem.* 25, 571–574
9 Kondō, S. *et al.* (1965) Destomycins A and B, two new antibiotics produced by *Streptomyces. J. Antibiot. Ser. A* 18, 38–42
10 Sasaki, T. *et al.* (1992) A new anthelmintic cyclodepsipeptide, PF1022A. *J. Antibiot. (Tokyo)* 45, 692–697
11 Harder, A. and von Samson-Himmelstjerna, G. (2002) Cyclooctadepsipeptides – a new class of anthelmintically active compounds. *Parasitol. Res.* 88, 481–488
12 Saeger, B. *et al.* (2001) Latrophilin-like receptor from the parasitic nematode *Haemonchus contortus* as target for the anthelmintic depsipeptide PF1022A. *FASEB J.* 15, 1332–1334
13 Hosoya, S. *et al.* (1952) Trichomycin, a new antibiotic produced by *Streptomyces hachijoensis* with trichomonadicidal and antifungal activity. *Jpn. J. Exp. Med.* 22, 505–509
14 Maeda, K. *et al.* (1953) A new antibiotic, azomycin. *J. Antibiot. Ser. A* 6, 182
15 Horie, H. (1956) Anti-trichomonas effect of azomycin. *J. Antibiot. (Tokyo)* 9, 168
16 Kano, H. and Ogata, K. (1957) Isoxazole derivatives. X. Synthesis of 5-methyl-3-sulfanilamidoisoxazole. *Ann. Rept. Shionogi Res. Lab.* 7, 1–5
17 Kim, H-S. *et al.* (2001) Synthesis and antimalarial activity of novel medium-sized 1,2,4,5-tetraoxacycloalkanes. *J. Med. Chem.* 44, 2357–2361
18 Kitade, Y. *et al.* (2003) Synthesis of 2-fluoronoraristeromycin and its inhibitory activity against *Plasmodium falciparum S*-adenosyl-L-homocysteine hydrolase. *Bioorg. Med. Chem. Lett.* 13, 3963–3965
19 Omura, S. and Crump, A. (2004) The life and times of ivermectin – a success story. *Nat. Rev. Microbiol.* 2, 984–989
20 Egerton, J.R. *et al.* (1979) Avermectins, new family of potent anthelmintic agents: efficacy of the B_{1a} component. *Antimicrob. Agents Chemother.* 15, 372–378
21 Burg, R.W. *et al.* (1979) Avermectins, new family of potent anthelmintic agents: producing organism and fermentation. *Antimicrob. Agents Chemother.* 15, 361–367
22 Takahashi, Y. *et al.* (2002) *Streptomyces avermectinius* sp. nov., an avermectin-producing strain. *Int. J. Syst. Evol. Microbiol.* 52, 2163–2168
23 Chabala, J.C. *et al.* (1980) Ivermectin, a new broad-spectrum antiparasitic agent. *J. Med. Chem.* 23, 1134–1136
24 Shoop, W. and Soll, M. (2002) Ivermectin, abamectin and eprinomectin. In *Macrocyclic Lactones in Antiparasitic Therapy* (Vercruysse, J. and Rew, R.S., eds), pp. 1–29, CABI Publishing
25 Richards, F.O. *et al.* (2001) Control of onchocerciasis today: status and challenges. *Trends Parasitol.* 17, 558–563
26 Richard-Lenoble, D. *et al.* (2003) Ivermectin and filariasis. *Fundam. Clin. Pharmacol.* 17, 199–203
27 Geary, T.G. (2005) Ivermectin 20 years on: maturation of a wonder drug. *Trends Parasitol.* 21, 530–532
28 Zaha, O. *et al.* (2002) Ivermectin in clinical practice. In *Macrolide Antibiotics. Chemistry, Biology, and Practice* (2nd edn) (Ōmura, S., ed.), pp. 403–419, Academic Press
29 Heukelbach, J. and Feldmeier, H. (2006) Scabies. *Lancet* 367, 1767–1774

30 Ōmura, S. (2002) Mode of action of avermectin. In *Macrolide Antibiotics. Chemistry, Biology, and Practice* (2nd edn) (Ōmura, S., ed.), pp. 571–576, Academic Press
31 Schinkel, A.H. *et al.* (1994) Disruption of the mouse *mdr1a* P-glycoprotein gene leads to a deficiency in the blood–brain barrier and to increased sensitivity to drugs. *Cell* 77, 491–502
32 Ikeda, H. *et al.* (2003) Complete genome sequence and comparative analysis of the industrial microorganism *Streptomyces avermitilis*. *Nat. Biotechnol.* 21, 526–531
33 Ōmura, S. *et al.* (1987) Jietacins A and B, new nematocidal antibiotics from a *Streptomyces* sp. Taxonomy, isolation, and physico-chemical and biological properties. *J. Antibiot. (Tokyo)* 40, 623–629
34 Ōmura, S. *et al.* (2001) An anthelmintic compound, nafuredin, shows selective inhibition of complex I in helminth mitochondria. *Proc. Natl. Acad. Sci. U. S. A.* 98, 60–62
35 Miyadera, H. *et al.* (2003) Atpenins, potent and specific inhibitors of mitochondrial complex II (succinate–ubiquinone oxidoreductase). *Proc. Natl. Acad. Sci. U. S. A.* 100, 473–477
36 Ōmura, S. *et al.* (1985) Anticoccidial activity of frenolicin B and its derivatives. *J. Antibiot. (Tokyo)* 38, 1447–1448
37 Crump, A. and Otoguro, K. (2005) Satoshi Ōmura: in pursuit of nature's bounty. *Trends Parasitol.* 21, 126–132
38 Otoguro, K. *et al.* (2003) *In vitro* and *in vivo* antimalarial activities of a non-glycosidic 18-membered macrolide antibiotic, borrelidin, against drug-resistant strains of Plasmodia. *J. Antibiot. (Tokyo)* 56, 727–729
39 Kita, K. and Takamiya, S. (2002) Electron transfer complexes in *Ascaris* mitochondria. *Adv. Parasitol.* 51, 95–131
40 Yamashita, T. *et al.* (2004) Rhodoquinone reaction site of mitochondrial complex I, in parasitic helminth, *Ascaris suum*. *Biochim. Biophys. Acta, (Bioenergetics)* 1608, 97–103
41 Amino, H. *et al.* (2003) Isolation and characterization of the stage-specific Cytochrome b small subunit (CybS) of *Ascaris suum* complex II from the aerobic respiratory chain of larval mitochondria. *Mol. Biochem. Parasitol.* 128, 175–186
42 Mitamura, T. *et al.* (2000) Serum factor governing intraerythrocytic development and cell cycle progression of *Plasmodium falciparum*. *Parasitol. Int.* 49, 219–229
43 Placpac, N.M. *et al.* (2004) Evidence that *Plasmodium falciparum* diacylglycerol acyltransferase is essential for intraerythrocytic proliferation. *Biochem. Biophys. Res. Commun.* 321, 1062–1068
44 Mitamura, T. and Placpac, N. (2003) Lipid metabolism in *Plasmodium falciparum*-infected erythrocyte: possible new targets for malaria chemotherapy. *Microbes Infect.* 5, 545–552
45 Müller, S. (2004) Redox and antioxidant systems of the malaria parasite *Plasmodium falciparum*. *Mol. Microbiol.* 53, 1291–1305
46 Komaki-Yasuda, K. *et al.* (2003) Disruption of the *Plasmodium falciparum* 2-Cys peroxiredoxin gene renders parasites hypersensitive to reactive oxygen and nitrogen species. *FEBS Lett.* 547, 140–144
47 Kawazu, S. *et al.* (2005) Roles of 1-Cys peroxiredoxin in heme detoxification in the human malaria parasite *Plasmodium falciparum*. *FEBS J.* 272, 1784–1791
48 Yano, K. *et al.* (2005) Expression of mRNAs and proteins for peroxiredoxins in *Plasmodium falciparum* erythrocytic stage. *Parasitol. Int.* 54, 35–41
49 Takashima, E. *et al.* (2001) Isolation of mitochondria from *Plasmodium falciparum* showing dihydroorotate dependent respiration. *Parasitol. Int.* 50, 273–278
50 Mi-ichi, F. *et al.* (2005) Parasite mitochondria as a target of chemotherapy: The inhibitory effect of licochalcone A on the Plasmodium falciparum respiratory chain. *Ann. N. Y. Acad. Sci.* 1056, 46–54
51 Gao, G. *et al.* (1999) Novel organization and sequences of five genes encoding all six enzymes for *de novo* pyrimidine biosynthesis in *Trypanosoma cruzi*. *J. Mol. Biol.* 285, 149–161
52 Aoki, T. (2003) Metabolism of parasitic protozoa. In *Progress of Medical Parasitology in Japan* (Vol. 7) (Otsuru, M. *et al.*, eds), pp. 175–191, Meguro Parasitological Museum
53 Annoura, T. *et al.* (2005) The origin of dihydroorotate dehydrogenase genes of kinetoplastids, with special reference to their biological significance and adaptation to anaerobic, parasitic conditions. *J. Mol. Evol.* 60, 113–127
54 Nara, T. *et al.* (2005) Inhibitory action of marine algae extracts on the *Trypanosoma cruzi* dihydroorotate dehydrogenase activity and on the protozoan growth in mammalian cells. *Parasitol. Int.* 54, 59–64
55 Sariego, I. *et al.* (2006) Genetic diversity and kinetic properties of *Trypanosoma cruzi* dihydroorotate dehydrogenase isoforms. *Parasitol. Int.* 55, 11–16
56 Inaoka, K. *et al.* (2005) Expression, purification, and crystallization of *Trypanosoma cruzi* dihydroorotate dehydrogenase complexed with orotate. *Acta Crystallogr. F61* 875–878
57 Nakajima-Shimada, J. *et al.* (2000) Inhibition of Fas-mediated apoptosis by *Trypanosoma cruzi* infection. *Biochim. Biophys. Acta* 1475, 175–183
58 Hashimoto, M. *et al.* (2005) *Trypanosoma cruzi* post-transcriptionally upregulates and exploits cellular FLIP for inhibition of death-inducing signal. *Mol. Biol. Cell* 16, 3521–3528
59 Nihei, C. *et al.* (2002) Trypanosome alternative oxidase as a target of chemotherapy. *Biochim. Biophys. Acta* 1587, 234–239
60 Yabu, Y. *et al.* (2006) Chemotherapeutic efficacy of ascofuranone in *Trypanosoma vivax*-infected mice without glycerol. *Parasitol. Int.* 55, 39–43
61 Nakamura, K. *et al.* (2005) Mutational analysis of the *Trypanosoma vivax* alternative oxidase: the $E(X)_6Y$ motif is conserved in both mitochondrial alternative oxidase and plastid terminal oxidase and is indispensable for enzyme activity. *Biochem. Biophys. Res. Commun.* 334, 593–600
62 Suzuki, T. *et al.* (2004) Direct evidence for cyanide insensitive quinol oxidase (alternative oxidase) in apicomplexan parasite *Cryptosporidium parvum*: phylogenetic and therapeutic implication. *Biochem. Biophys. Res. Commun.* 313, 1044–1052
63 Nozaki, T. *et al.* (2005) Sulfur-containing amino acid metabolism in parasitic protozoa. *Adv. Parasitol.* 60, 1–100
64 Saito-Nakano, Y. *et al.* (2004) Rab5-associated vacuoles play a unique role in phagocytosis of the enteric protozoan parasite *Entamoeba histolytica*. *J. Biol. Chem.* 279, 49497–49507
65 Loftus, B. *et al.* (2005) The genome of the protist parasite *Entamoeba histolytica*. *Nature* 433, 865–868
66 Okada, M. *et al.* (2005) Proteomic analysis of phagocytosis in the enteric protozoan parasite *Entamoeba histolytica*. *Eukaryot. Cell* 4, 827–831
67 Nakada-Tsukui, K. *et al.* (2005) A retromerlike complex is a novel Rab7 effector that is involved in the transport of the virulence factor cysteine protease in the enteric protozoan parasite *Entamoeba histolytica*. *Mol. Biol. Cell* 16, 5294–5303
68 Okada, M. and Nozaki, T. (2006) New insights into molecular mechanisms of phagocytosis in *Entamoeba histolytica* by proteomic analysis. *Arch. Med. Res.* 37, 244–251
69 Nozaki, T. and Nakada-Tsukui, K. (2006) Membrane trafficking as a virulence mechanism of the enteric protozoan parasite *Entamoeba histolytica*. *Parasitol. Res.* 98, 179–183
70 Makioka, A. *et al.* (2006) Characterization of protein geranylgeranyltransferase I from the enteric protist *Entamoeba histolytica*. *Mol. Biochem. Parasitol.* 145, 216–225
71 Yoneda, S. *et al.* (1977) Some observations on the effect of Ro 7-1051 on *Trypanosoma cruzi*, particularly in cell culture. *Experientia* 33, 1201–1202
72 Cosar, C. and Julou, L. (1959) Activity of 1-(2-hydroxyethyl)-2-methyl-5-nitroimidazole (RP 8823) in experimental *Trichomonas vaginalis* infections. *Ann. Inst. Pasteur* 96, 238–241

Available online at www.sciencedirect.com
ScienceDirect
Biochemical and Biophysical Research Communications 358 (2007) 130–135
BBRC
www.elsevier.com/locate/ybbrc

Relationship between reactive oxygen species and heme metabolism during the differentiation of Neuro2a cells

Noriko Shinjyo, Kiyoshi Kita *

Department of Biomedical Chemistry, Graduate School of Medicine, The University of Tokyo, 7-3-1 Hongo, Bunkyo-ku, Tokyo 113 0033, Japan

Received 31 March 2007
Available online 19 April 2007

Abstract

Although neuronal cells are highly vulnerable to oxidative stress, recent studies suggest that production of reactive oxygen species (ROS) increases during and is essential for neuronal differentiation. In addition, we have previously found that heme biosynthesis is up-regulated during retinoic acid-induced differentiation of Neuro2a cells. In the current study, we showed that this up-regulation of heme biosynthesis during differentiation is ROS-dependent. Furthermore, we found that ROS-dependent induction of heme oxygenase, which degrades heme and acts as an anti-oxidant, and catalase, another anti-oxidant enzyme that contains heme as a prosthetic group, occurs during differentiation. These results suggest that heme biosynthesis following the degradation of heme protects Neuro2a cells from oxidative stress caused by ROS during differentiation.

Keywords: Neuron; Differentiation; ROS; Heme; Heme oxygenase; Catalase

Heme is an essential prosthetic group in many proteins and plays a regulatory role in cells [1]. Several groups have reported that heme is important in the nervous system. For example, a deficiency in heme causes neuronal cell death and the suppression of key neuronal genes [2,3]. Also, altered heme metabolism may be related to aging and Alzheimer's disease [4].

In addition, heme is a substrate of heme oxygenase (HO), which degrades heme to biliverdin, CO, and Fe^{2+}. Bilirubin, metabolite of biliverdin, is a potent radical scavenger and protects neuronal cells from oxidative stress [5]. In a previous study, we found that heme biosynthesis is up-regulated during retinoic acid (RA)-induced differentiation of Neuro2a cells [6], but we did not determine the significance or identify the regulatory mechanism of this up-regulation.

Recent reports show that neuronal cells produce high levels of ROS [7,8]. ROS, which includes free radicals and peroxides, are generally highly reactive molecules and could cause significant damage to the neuronal cells. It is therefore expected that anti-oxidant systems are indispensable for neuronal survival. In general, cells possess several strategies to avoid damage by ROS, including ROS-degrading enzymes and low-molecular weight anti-oxidants. Two of the enzymatic systems, HO and catalase, require heme for activity.

In this study, we examined the relationship between the up-regulation of heme biosynthesis and ROS production during the differentiation of Neuro2a cells [6]. We specifically focused on the role of HO and catalase in the relationship between heme metabolism and ROS.

Materials and methods

Cell culture. Neuro2a cells were cultured as described previously [6] in Dulbecco's modified Eagle's medium (DMEM; Sigma-Aldrich, St. Louis,

Abbreviations: ALAS-1, 5-aminolevulinic acid synthase-1; 3-AT, 3-aminotriazole; CPG, coproporphyrinogen; DSP, downstream primer; HO, heme oxygenase; NAC, *N*-acetyl cysteine; PMP70, peroxisomal membrane protein 70; RA, retinoic acid; ROS, reactive oxygen species; SA, succinyl-acetone; USP, upstream primer; ZnPP IX, zinc protoporphyrin IX.

* Corresponding author. Fax: +81 3 5841 3444.
E-mail address: kitak@m.u-tokyo.ac.jp (K. Kita).

0006-291X/$ - see front matter © 2007 Elsevier Inc. All rights reserved.
doi:10.1016/j.bbrc.2007.04.071

MO, USA) supplemented with 10% (v/v) fetal bovine serum (FBS; Gibco BRL Life Technologies, Paisley, Scotland), 100 U/ml penicillin, 100 μg/ml streptomycin, and 292 μg/ml glutamine at 37 °C in a humidified 5% (v/v) CO_2 incubator. Differentiation was induced by treating the cells with 20 μM RA in DMEM containing 2% (v/v) FBS.

Detection of intracellular H_2O_2. Cells were seeded on coverslips (Grace Bio-Lab., Bend, OR) and incubated as described above (see Cell culture). H_2O_2 was detected using the fluorescent probe BES–H_2O_2 (Commercial name) (Wako, Nagoya Japan), which is converted to a fluorescent product by reaction with H_2O_2. The medium was replaced with fresh medium containing 10 μM BES-H_2O_2 with or without 10 mM *N*-acetyl cysteine (NAC) and incubated for 15 min at 37 °C in a humidified 5% (v/v) CO_2 incubator. Prior to observation, the BES-H_2O_2-containing medium was removed, and the cells on the coverslips were washed with phosphate-buffered saline (pH 7.4). Next pre-warmed medium (2% FBS/DMEM) without BES-H_2O_2 was added, and the fluorescence was detected using a NIKON ECLIPSE E600 fluorescence microscope with a 465- to 495-nm excitation filter, a 505-nm dichroic mirror, and a 515- to 555-nm emission filter.

Detection of peroxisomes by immunofluorescence microscopy. Peroxisomes were detected using a Select Alexa Fluor 488 Peroxisome Labeling kit (Molecular probes), which detects peroxisomal membrane protein 70 (PMP70). Cells were grown on coverslips, and peroxisome staining was performed according to the manufacturer's instructions. Fluorescence from Alexa Fluor 488 was detected using a NIKON ECLIPSE E600 fluorescence microscope as described above (see Detection of intracellular H_2O_2).

Quantitative real-time PCR. Total RNA was isolated from cells using TRIzol (Invitrogen, Carlsbad, CA, USA) according to the manufacturer's protocol. RNA was reverse-transcribed, and complementary DNAs were synthesized using an oligo (dT) primer. Real-time PCR was performed using a LC real-time PCR apparatus (Roche Diagnostics, Mannheim, Germany) and a Quantitect SYBR-Green RT-PCR Kit (Qiagen, Hilden, Germany) in a 20-μl volume containing 0.5 μM of each upstream primer (USP) and downstream primer (DSP) according to the manufacturer's instructions. The primers used were as follows: for β-actin, β-actin-USP (5′-tggaatcctgtggcatccatgaaac-3′), and β-actin-DSP (5′-taaaacgcagctcag-taacagtccg-3′); for 5-aminolevulinic acid synthase-1 (ALAS-1), ALAS-1-USP (5′-gtcaagcttctgaggc-3′), and ALAS-1-DSP (5′-cctggtcatcaactc-3′); for coproporphyrinogen oxidase (CPG oxidase, EC 1.3.3.3), CPG oxidase-USP (5′-ctccaggatccaggatc-3′), and CPG oxidase-DSP (5′-cctttggatggcg-caac-3′); for porphobilinogen deaminase (PBG deaminase, EC 2.5.1.61), PBG deaminase-USP (5′-ccgtagcagtgcatacagtg-3′), and PBG deaminase-USP (5′-ctggatggtggcctgcatag-3′); for catalase, catalase-USP (5′-ccagtgcgctgtagatg-3′) and catalase-DSP (5′-caatgttctcacacaggc-3′); for HO, HO-1-USP (5′-gacacctgaggtcaagc-3′) and HO-1-DSP (5′-ctctgacgaagtgacg-3′). The PCR was carried out as follows: initial denaturation at 95 °C for 10 min, followed by 40 cycles of denaturation for 10 s at 95 °C, elongation for 20 s (60 °C for β-actin and PBG deaminase; 52 °C for ALAS-1, and 58 °C for CPG oxidase, catalase, and HO-1), and annealing for 10 s at 72 °C. The mRNA levels were normalized according to the level of β-actin mRNA.

Measurement of catalase activity. Collected cells were suspended in potassium phosphate (50 mM) buffer (pH 7.0) containing 1 mM EDTA, homogenized, and centrifuged at 10,000*g* for 15 min at 4 °C. Catalase activities in the supernatants were measured using an Amplex Red reagent-based H_2O_2 detection system (Amplex Red Catalase Assay Kit, Molecular Probes) according to the manufacturer's instructions.

Measurement of HO activity. HO activity was measured by the bilirubin generation method [9,10]. In brief, cells were collected by centrifugation (1000*g* for 10 min at 4 °C), and the cell pellet was suspended in a buffer of 2 mM $MgCl_2$ in 100 mM potassium phosphate (pH 7.4), sonicated on ice, and centrifuged at 18,800*g* for 10 min at 4 °C. The supernatant was added to the reaction mixture (100 μl), which contained rat liver cytosol (0.5 mg/ml), hemin (20 μM), glucose-6-phosphate (2 mM), glucose-6-phosphate dehydrogenase (0.2 U), and NADPH (0.8 mM), and incubated for 1 h at 37 °C in the dark. The formed bilirubin was extracted with 300 μl of chloroform, and the change in optical density between 464 and 530 nm was measured (extinction coefficient = 40 mM^{-1} cm^{-1} for bilirubin).

Statistical analysis. Each experiment was performed three times. The data were plotted as the means ± SD. Student's *t*-test was used for comparisons. Differences were considered significant at $P < 0.01$ or 0.05 as indicated in the figure legends.

Results

ROS production during differentiation of Neuro2a cells'

Because neuronal cells may produce high levels of ROS [7,8], we examined whether Neuro2a cells produce ROS during RA-induced differentiation. In these experiments, we used the probe BES-H_2O_2 to measured the production of H_2O_2, which is a relatively stable molecule and thought to be a major form ROS [8].

We found that the fluorescence intensity produced by BES-H_2O_2 was significantly higher in RA-treated differentiating cells than in untreated control cells (Supplement 1a). The fluorescence was almost completely abolished by inclusion of the radical scavenger NAC (Supplement 1b), confirming that the observed fluorescence was ROS-dependent. The higher fluorescence levels were observed from around 6 h after the treatment with RA and continued thereafter (data not shown), indicating that ROS is produced in differentiating Neuro2a cells.

Effect of the radical scavenger NAC on the expression of heme biosynthetic enzymes in Neuro2a cells during RA-induced differentiation

Because we previously observed that heme biosynthesis is up-regulated during differentiation of Neuro2a cells [6] and because heme is essential for the activity of anti-oxidative enzymes, we postulated that the up-regulation of heme biosynthesis is related to the increase in ROS levels during differentiation. Therefore, we examined the effect of the radical scavenger NAC on heme biosynthesis.

We first measured the effect of NAC on the mRNA levels for rate-limiting enzymes, namely, ALAS-1 and CPG oxidase, which we previously found to be up-regulated in Neuro2a cells during RA-induced differentiation, and on the level of PBG deaminase, which did not change significantly during differentiation [6]. As shown in Fig. 1, the up-regulation of mRNA levels for ALAS-1 and CPG oxidase by RA was inhibited by NAC, whereas the mRNA level for PBG deaminase was not affected by RA or NAC. This result suggests that the up-regulation of heme biosynthesis during Neuro2a differentiation is ROS-dependent.

Alteration in the level of HO-1 mRNA and HO enzymatic activity during RA-induced differentiation in Neuro2a cells

HO plays an anti-oxidative role by converting heme into the anti-oxidant bilirubin. HO-1, the inducible form of HO,

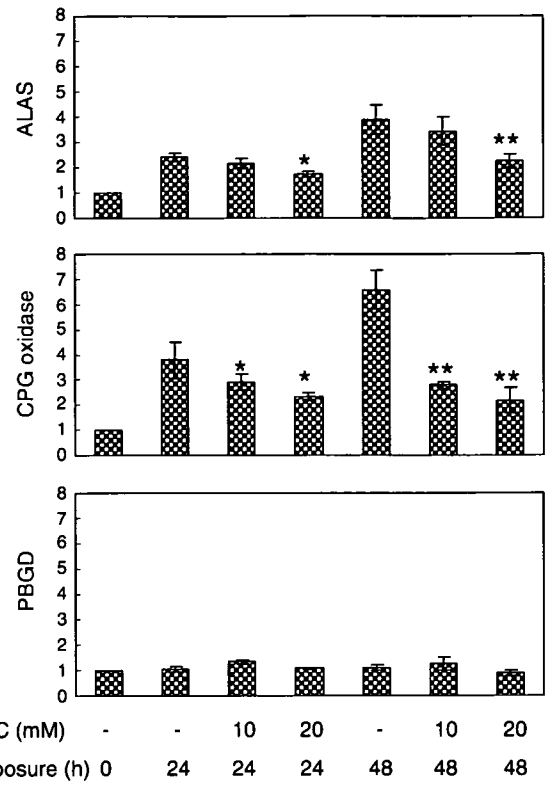

Fig. 1. Effect of NAC on the mRNA levels for heme biosynthetic enzymes. Cells were exposed to RA in the presence or absence of NAC (10 and 20 mM). The mRNA levels for heme biosynthetic enzymes ALAS-1, CPG oxidase, and PBG deaminase were measured using quantitative RT-PCR. Results represent the means ± SD ($n = 3$). $^{*}P < 0.05$ vs. 24 h, $^{**}P < 0.05$ vs. 48 h without NAC.

responds to various stimuli including ROS [11,12]. Because our results suggested that ROS up-regulates heme biosynthetic enzymes, we suspected that ROS increases the demand for bilirubin and therefore heme. For this reason, we examined the effect of RA on the level of HO-1 mRNA and HO enzymatic activity in Neuro2a cells.

We treated the Neuro2a cells for up to 48 h with RA, isolated total RNA, and examined the level of HO-1 mRNA by RT-PCR. As shown in Fig. 2A, the level of HO-1 mRNA increased during differentiation and was approximately 10-fold higher than in untreated control cells 12 h after the induction of differentiation with RA. The level of HO-1 mRNA did not increase thereafter. We also examined the effect of the radical scavenger NAC (10 mM) on the changes in HO-1 mRNA levels. NAC greatly suppressed the increase in HO-1 mRNA levels during differentiation (Fig. 2A). We further measured the HO enzymatic activity in Neuro2a cells exposed to RA for 12 h in the presence or absence of 10 mM NAC (Fig. 2B). HO activity increased after the induction of differentiation, and the activation of HO was greatly reduced by NAC, similar to the changes in the HO-1 mRNA level (Fig. 2A). These results show that HO is activated through the ROS-dependent induction of HO-1 during RA-induced differentiation of Neuro2a cells.

Alteration in the level of catalase in Neuro2a cells during RA-induced differentiation

Catalase is a heme-containing enzyme that catalyzes the decomposition of hydrogen peroxide (H_2O_2) to water and oxygen. Because catalase is an important anti-oxidative enzyme, we examined whether it is also induced during differentiation in Neuro2a cells.

Differentiation was induced in the presence or absence of NAC, and catalase mRNA levels were examined by RT-PCR. As shown in Fig. 2C, the expression of catalase was increased during differentiation, and this induction was suppressed by NAC. We also examined the changes in the enzymatic activity of catalase (Fig. 2D). Catalase was activated approximately 2.5-fold after 48 h of RA-induced differentiation. The activation of catalase was suppressed by NAC. These results suggested that during differentiation, like HO, catalase is activated by ROS. Compared with its effects on HO induction, NAC had a moderate effect on catalase induction. Thus, 10 mM NAC was apparently not sufficient to obtain strong inhibition, although the inhibition was more obvious at 20 mM NAC (Fig. 2D).

Effect of the heme biosynthesis inhibitor succinyl-acetone (SA) on catalase activity and peroxisomal distribution in Neuro2a cells

Because catalase contains heme as a prosthetic group, heme biosynthesis may be essential for the activation of catalase. Thus, we examined whether the inhibition of heme biosynthesis affects the activation of catalase during RA-induced differentiation. Differentiation was induced in the presence or absence of 1 mM SA, an inhibitor of heme biosynthesis, and the catalase activity was measured in cell lysates. We found that SA prevented the increase in catalase activity (Fig. 3).

Catalase is a peroxisomal protein in animal cells, and its importance in the detoxification of ROS has been described previously [13]. In addition, peroxisomes are known to be critical for the function of neurons and the nervous system [14]. Therefore, we examined whether the administration of SA affects the distribution of peroxisomes. Differentiation was induced in the presence or absence of 1 mM SA, and the peroxisomes were stained using an antibody against the peroxisomal protein PMP70. Peroxisomes were abnormally distributed in SA-treated cells. Specifically, we observed many aggregated or dot-like signals in the neurites of SA-treated cells (Supplement 2). Similar changes were also observed in cells treated with the catalase inhibitor 3-aminotriazole (3-AT) (Supplement 3).

Effect of the HO inhibitor zinc protoporphyrin IX (ZnPP IX) on the level of ALAS-1 mRNA in Neuro2a cells

As shown in Fig. 2A, the induction of HO-1 mRNA occurred in the early stage of differentiation (6–12 h) before

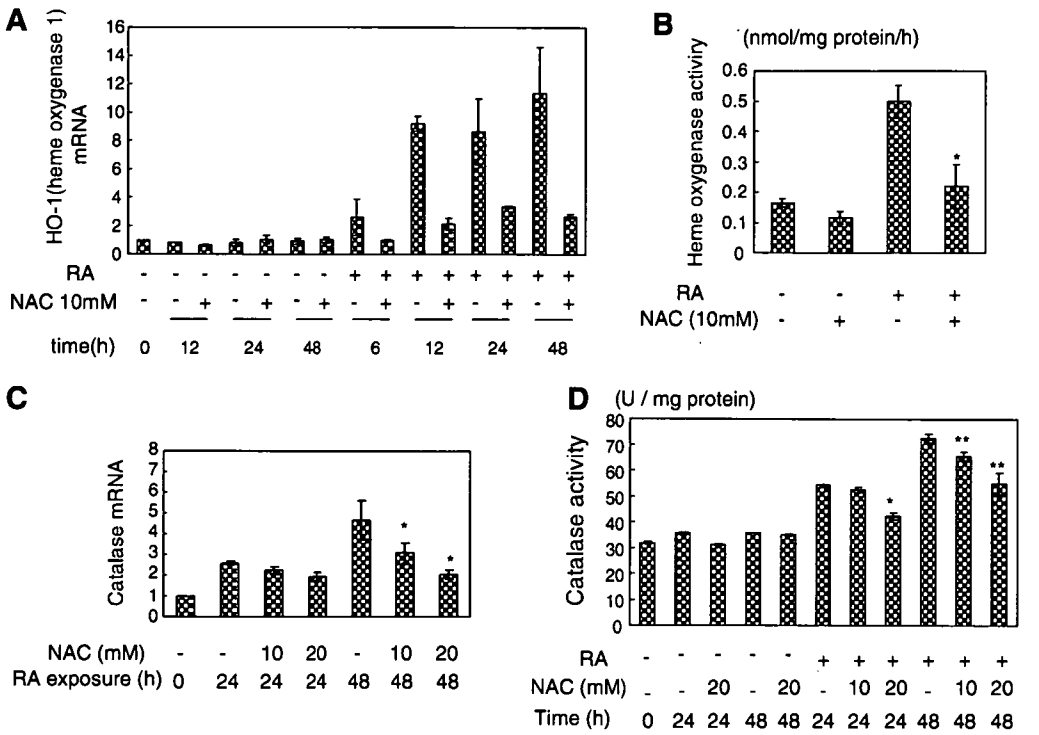

Fig. 2. (A) Changes in the level of HO-1 mRNA during RA-induced differentiation in the presence or absence of NAC. Cells were exposed to RA with or without 10 mM NAC, and HO-1 mRNA levels were measured by quantitative RT-PCR. Signals were normalized by the signal for β-actin mRNA, and the values relative to those at 0 h are presented. (B) HO activity in the presence or absence of NAC. Following a 12 h exposure to RA in the presence or absence of 10 mM NAC, cells were lysed, and HO activity was measured in the cell lysates. Results represent the means ± SD ($n = 3$). The statistical significance was evaluated using Student's t-test ($^{*}P < 0.01$ vs. 12 h with RA). (C) Changes in the level of catalase mRNA during differentiation in the presence or absence of NAC. Differentiation of Neuro2a cells was induced with RA in the presence or absence of NAC (10 and 20 mM). The level of mRNA for catalase was measured by quantitative RT-PCR. Results represent the means ± SD ($n = 3$). $^{*}P < 0.05$ vs. 24 h, $^{**}P < 0.05$ vs. 48 h without NAC. (D) Changes in catalase activity during differentiation in the presence or absence of NAC. Cell lysates were prepared, and catalase activity was measured using Amplex Red. Results represent the means ± SD ($n = 3$). $^{*}P < 0.01$ vs. 24 h, $^{**}P < 0.01$ vs. 48 h without NAC.

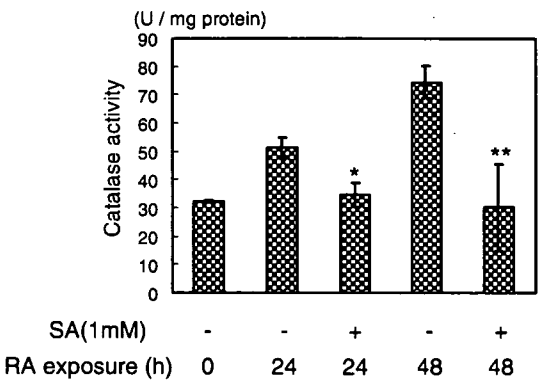

Fig. 3. Effect of SA on the changes in catalase activity. Cells were treated with RA in the presence or absence of 1 mM SA, and catalase activity was measured in cell lysates. Results represent the means ± SD ($n = 3$). $^{*}P < 0.01$ vs. 24 h, $^{**}P < 0.01$ vs. 48 h without SA.

the up-regulation of heme biosynthesis (~48 h) [6], indicating that the HO-1 is a primary target of ROS. To clarify the relationship between the up-regulation of heme biosynthesis and the induction of HO activity, we examined the effect of ZnPP IX, a competitive inhibitor of HO, on the induction of ALAS-1. We found that the increase in ALAS-1 mRNA was significantly reduced by ZnPP IX (Fig. 4A), although the mRNA encoding another heme biosynthetic enzyme, CPG oxidase, was not affected by ZnPP IX (data not shown). ZnPP IX caused a significant reduction in the level of ALAS-1 mRNA at concentrations above 1 μM, which corresponded with the dose-dependence of the effects of ZnPP IX on HO activity (Fig. 4B).

Discussion

In this study, we examined the relationship between ROS and heme metabolism during the differentiation of Neuro2a cells. It has been suggested that heme plays an essential role in the differentiation of neuronal cells [2–4], but the functions of heme are diverse [15] and their significance in neuronal cells has not been fully elucidated. Based on our previous observation that heme biosynthesis is up-regulated during the differentiation of Neuro2a cells [6], our current results suggest that this is related to the activation of anti-oxidative enzymes HO and catalase.

Catalase is one of the major proteins in peroxisomes [16]. Because catalase contains heme as an essential pros-

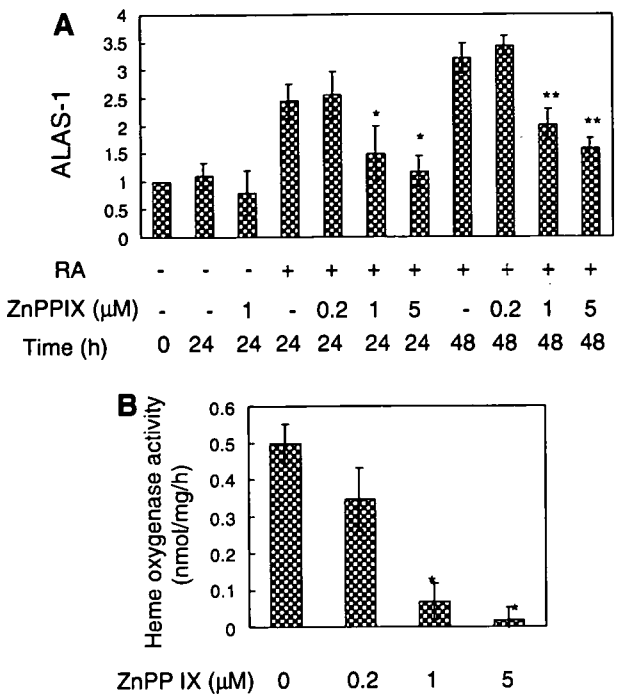

Fig. 4. (A) Effect of ZnPP IX on the level of mRNA for the heme biosynthetic enzyme ALAS-1. Cells were treated with ZnPP IX (0.2, 1, and 5 mM) and the mRNA level for ALAS-1 was measured by quantitative RT-PCR. Results represent the means ± SD ($n = 3$). $^{*}P < 0.01$ vs. 24 h, $^{**}P < 0.01$ vs. 48 h without ZnPP IX. (B) Effect of ZnPP IX on HO activity. Cells were exposed to RA for 12 h in the presence or absence of ZnPP IX, and HO activity was measured in cell lysates. The activity was presented as nmol bilirubin/mg protein/h. Results represent the means ± SD ($n = 3$). $^{*}P < 0.01$ vs. without ZnPP IX.

thetic group, our finding of simultaneous ROS-dependent up-regulation of heme biosynthesis and catalase activity suggests that heme biosynthesis plays an indispensable role in catalase activation. Thus, oxidative damage due to a deficiency in catalase activity could explain the abnormal distribution of peroxisomes observed in SA-treated cells (Fig. 3B). In fact, in the nematode *Caenorhabditis elegans* [13,17], a lack of peroxisomal catalase causes a progeric phenotype and the appearance of aggregated peroxisomes with altered morphologies [13].

Another important finding in this study was that HO-1 is induced by a ROS-dependent mechanism during differentiation. Analysis of the changes in the level of HO-1 mRNA indicated that this enzyme is induced during the very early stage of differentiation and before the induction of catalase and heme biosynthetic enzymes. HO is an anti-oxidative enzyme, and its inducible form, HO-1, is an integral part of the antioxidant system in cells [18] and is up-regulated by a variety of factors, including ROS [11,12]. It is likely that HO-1 induction is the primary target of ROS and that it contributes to the up-regulation of heme biosynthesis, possibly through the consumption of heme [19]. This may help meet demand for heme needed for catalase activation. In fact, the up-regulation of ALAS-1 expression was suppressed by the HO inhibitor ZnPP IX but unaffected by the catalase inhibitor 3-AT (data not shown).

In this report, we investigated the relationship between ROS and heme metabolism during RA-induced differentiation of Neuro2a cells. Previous reports have demonstrated that ROS participate in the differentiation of nonneuronal cells and that NADPH oxidase helps produce ROS [20,21]. Elevation of the level of ROS also seems to be a common phenomenon in neuronal differentiation [7,8], although the source of ROS and the signaling mechanism leading to neuronal differentiation remains to be clarified. RA is essential not only for neuronal differentiation but also for neuronal regeneration [22,23]. Therefore, the findings in this study might also be relevant to neuronal regeneration.

Acknowledgments

This study was supported by a grant-in-aid for scientific research on priority areas, 21st Century COE program and for Creative Scientific Research from the Japanese Ministry of Education, Science, Culture, and Sports (13226015, 13854011, 17209013, 17590368, 18073004, and 18GS0314).

Appendix A. Supplementary data

Supplementary data associated with this article can be found, in the online version, at doi:10.1016/j.bbrc.2007.04.071.

References

[1] M.A. Gilles-Gonzalez, G. Gonzalez, Heme-based sensors: defining characteristics, recent developments, and regulatory hypotheses, J. Inorg. Biochem. 99 (2005) 1–22.
[2] Y. Zhu, T. Hon, W. Ye, L. Zhang, Heme deficiency interferes with the Ras-mitogen-activated protein kinase signaling pathway and expression of a subset of neuronal genes, Cell Growth. Differ. 13 (2002) 431–439.
[3] A. Sengupta, T. Hon, L. Zhang, Heme deficiency suppresses the expression of key neuronal genes and causes neuronal cell death, Brain Res. Mol. Brain Res. 137 (2005) 23–30.
[4] H. Atamna, W.H. Frey 2nd, A role for heme in Alzheimer's disease: heme binds amyloid beta and has altered metabolism, Proc. Natl. Acad. Sci. USA 101 (2004) 11153–11158.
[5] A. Kaizaki, S. Tanaka, K. Ishige, S. Numazawa, T. Yoshida, The neuroprotective effect of heme oxygenase (HO) on oxidative stress in HO-1 siRNA-transfected HT22 cells, Brain Res. 1108 (2006) 39–44.
[6] N. Shinjyo, K. Kita, Up-regulation of heme biosynthesis during differentiation of Neuro2a cells, J. Biochem. (Tokyo) 139 (2006) 373–381.
[7] M. Tsatmali, E.C. Walcott, K.L. Crossin, Newborn neurons acquire high levels of reactive oxygen species and increased mitochondrial proteins upon differentiation from progenitors, Brain Res. 1040 (2005) 137–150.
[8] K. Suzukawa, K. Miura, J. Mitsushita, J. Resau, K. Hirose, R. Crystal, T. Kamata, Nerve growth factor-induced neuronal differentiation requires generation of Rac1-regulated reactive oxygen species, J. Biol. Chem. 275 (2000) 13175–13178.
[9] R.K. Kutty, M.D. Maines, Oxidation of heme *c* derivatives by purified heme oxygenase: evidence for the presence of one molecular

species of heme oxygenase in the rat liver, J. Biol. Chem. 257 (1982) 9944–9952.
[10] J. Patel, N. Manjappa, R. Bhat, P. Mehrotra, M. Bhaskaran, P.C. Singhal, Role of oxidative stress and heme oxygenase activity in morphine-induced glomerular epithelial cell growth, Am. J. Physiol. Renal Physiol. 285 (2003) F861–F869.
[11] S.H. Chang, J. Garcia, J.A. Melendez, M.S. Kilberg, A. Agarwal, Haem oxygenase 1 gene induction by glucose deprivation is mediated by reactive oxygen species via the mitochondrial electron-transport chain, Biochem. J. 371 (2003) 877–885.
[12] J.H. Yi, A.S. Hazell, *N*-acetylcysteine attenuates early induction of heme oxygenase-1 following traumatic brain injury, Brain Res. 1033 (2005) 13–19.
[13] O.I. Petriv, R.A. Rachubinski, Lack of peroxisomal catalase causes a progeric phenotype in *Caenorhabditis elegans*, J. Biol. Chem. 279 (2004) 19996–20001.
[14] P.L. Faust, D. Banka, R. Siriratsivawong, V.G. Ng, T.M. Wikander, Peroxisome biogenesis disorders: the role of peroxisomes and metabolic dysfunction in developing brain, J. Inherit. Metab. Dis. 28 (2005) 369–383.
[15] A.S. Tsiftsoglou, A.I. Tsamadou, L.C. Papadopoulou, Heme as key regulator of major mammalian cellular functions: molecular, cellular, and pharmacological aspects, Pharmacol. Ther. 111 (2006) 327–345.
[16] C. Causeret, M. Bentejac, M. Bugaut, Proteins and enzymes of the peroxisomal membrane in mammals, Biol. Cell. 77 (1993) 89–104.
[17] C.S. Wood, J.I. Koepke, H. Teng, K.K. Boucher, S. Katz, P. Chang, L.J. Terlecky, I. Papanayotou, P.A. Walton, S.R. Terlecky, Hypocatalasemic fibroblasts accumulate hydrogen peroxide and display age-associated pathologies, Traffic 7 (2006) 97–107.
[18] K. Chen, K. Gunter, M.D. Maines, Neurons overexpressing heme oxygenase-1 resist oxidative stress-mediated cell death, J. Neurochem. 75 (2000) 304–313.
[19] P.D. Drew, I.Z. Ades, Regulation of the stability of chicken embryo liver delta-aminolevulinate synthase mRNA by hemin, Biochem. Biophys. Res. Commun. 162 (1989) 102–107.
[20] J. Li, M. Stouffs, L. Serrander, B. Banfi, E. Bettiol, Y. Charnay, K. Steger, K.H. Krause, M.E. Jaconi, The NADPH oxidase NOX4 drives cardiac differentiation: Role in regulating cardiac transcription factors and MAP kinase activation, Mol. Biol. Cell. 17 (2006) 3978–3988.
[21] M. Ushio-Fukai, R.W. Alexander, Reactive oxygen species as mediators of angiogenesis signaling: role of NAD(P)H oxidase, Mol. Cell. Biochem. 264 (2004) 85–97.
[22] S. Jacobs, D.C. Lie, K.L. DeCicco, Y. Shi, L.M. DeLuca, F.H. Gage, R.M. Evans, Retinoic acid is required early during adult neurogenesis in the dentate gyrus, Proc. Natl. Acad. Sci. USA 103 (2006) 3902–3907.
[23] J. Mey, New therapeutic target for CNS injury? The role of retinoic acid signaling after nerve lesions, J. Neurobiol. 66 (2006) 757–779.

Available online at www.sciencedirect.com
ScienceDirect
Parasitology International 57 (2008) 54–61
www.elsevier.com/locate/parint

Change of subunit composition of mitochondrial complex II (succinate–ubiquinone reductase/quinol–fumarate reductase) in *Ascaris suum* during the migration in the experimental host

Fumiko Iwata [a,b], Noriko Shinjyo [a], Hisako Amino [a], Kimitoshi Sakamoto [a], M. Khyrul Islam [c], Naotoshi Tsuji [c], Kiyoshi Kita [a,*]

[a] *Department of Biomedical Chemistry, Graduate School of Medicine, The University of Tokyo, 7-3-1 Hongo, Bunkyo-ku, Tokyo 113 0033, Japan*
[b] *Department of Molecular and Cellular Physiology, Graduate School of Comprehensive Human Sciences, University of Tsukuba, Tsukuba, Japan*
[c] *Laboratory of Parasitic Diseases, National Institute of Animal Health, National Agriculture Research Organization, Tsukuba, Japan*

Received 13 July 2007; received in revised form 11 August 2007; accepted 16 August 2007
Available online 25 August 2007

Abstract

The mitochondrial metabolic pathway of the parasitic nematode *Ascaris suum* changes dramatically during its life cycle, to adapt to changes in the environmental oxygen concentration. We previously showed that *A. suum* mitochondria express stage-specific isoforms of complex II (succinate–ubiquinone reductase: SQR/quinol–fumarate reductase: QFR). The flavoprotein (Fp) and small subunit of cytochrome *b* (CybS) in adult complex II differ from those of infective third stage larval (L3) complex II. However, there is no difference in the iron–sulfur cluster (Ip) or the large subunit of cytochrome *b* (CybL) between adult and L3 isoforms of complex II. In the present study, to clarify the changes that occur in the respiratory chain of *A. suum* larvae during their migration in the host, we examined enzymatic activity, quinone content and complex II subunit composition in mitochondria of lung stage L3 (LL3) *A. suum* larvae. LL3 mitochondria showed higher QFR activity (~160 nmol/min/mg) than mitochondria of *A. suum* at other stages (L3: ~80 nmol/min/mg; adult: ~70 nmol/min/mg). Ubiquinone content in LL3 mitochondria was more abundant than rhodoquinone (~1.8 nmol/mg versus ~0.9 nmol/mg). Interestingly, the results of two-dimensional bule-native/sodium dodecyl sulfate polyacrylamide gel electrophoresis analyses showed that LL3 mitochondria contained larval Fp (Fp^L) and adult Fp (Fp^A) at a ratio of 1:0.56, and that most LL3 CybS subunits were of the adult form ($CybS^A$). This clearly indicates that the rearrangement of complex II begins with a change in the isoform of the anchor CybS subunit, followed by a similar change in the Fp subunit.

Keywords: *Ascaris suum* lung-stage L3 (LL3); Complex II; Quinone; NADH–fumarate reductase; Quinol–fumarate reductase (QFR); Oxidative stress

1. Introduction

During the life cycle of the parasitic nematode *Ascaris suum*, it transitions from aerobic to anaerobic metabolism in parallel with changes in the environmental oxygen concentration (Fig. 1) [1–6]. In aerobic metabolism, which is used by *A. suum* larvae during their development from fertilized egg to third stage larvae (L3), phosphoenolpyruvate (PEP) is converted to pyruvate by pyruvate kinase, and pyruvate is converted to CO_2 and H_2O via the tricarboxylic acid (TCA) cycle, generating a large amount of ATP by aerobic oxidative phosphorylation [7]. Adult *A. suum* worms, which live in a low-oxygen environment, use the anaerobic phosphoenolpyruvate carboxykinase (PEPCK)-

Abbreviations: Fp, flavoprotein subunit; Ip, iron–sulfur cluster subunit; CybL, large subunit of cytochrome *b*; CybS, small subunit of cytochrome *b*; Fp^L, larval Fp; Fp^A, adult Fp; $CybS^L$, larval CybS; $CybS^A$, adult CybS; L3, third stage larva; LL3, lung stage L3; SDH, succinate dehydrogenase; SQR, succinate–ubiquinone reductase; QFR, quinol–fumarate reductase; UQ, ubiquinone; dUQ, decyl UQ; RQ, rhodoquinone; dRQ, decyl RQ; HPLC, high performance liquid chromatography; BN-PAGE, blue-native polyacrylamide gel electrophoresis; SDS-PAGE, sodium dodecyl sulfate-PAGE; CBB, Coomassie brilliant blue.

* Corresponding author. Tel.: +81 3 5841 3526; fax: +81 3 5841 3444.
E-mail address: kitak@m.u-tokyo.ac.jp (K. Kita).

1383-5769/$ - see front matter © 2007 Elsevier Ireland Ltd. All rights reserved.
doi:10.1016/j.parint.2007.08.002

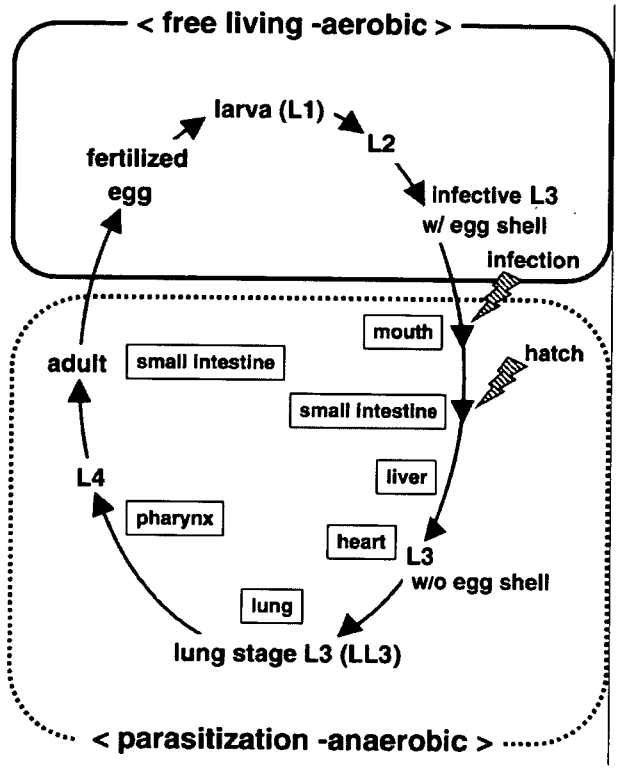

Fig. 1. Life cycle of *Ascaris suum*. Fertilized eggs grow to infective L3 under aerobic environment. Infective L3 larvae are ingested by the host, reach the small intestine and hatch there. Afterwards, larvae migrate into the host body (liver, heart, lung, pharynx), and finally migrate back to the small intestine and become adults. In the host small intestine, the oxygen concentration is only 2.5 to 5% of that of the exogenous environment [12]. w/, with; w/o, without.

succinate pathway. In the first step in the PEPCK-succinate pathway, PEPCK fixes CO_2 to PEP in the cytosol, to form oxaloacetate. This oxaloacetate is then reduced to malate, which is dismutated in mitochondria. Then, fumarate hydratase converts the malate to fumarate, which is reduced by the quinol–fumarate reductase (QFR) activity of complex II; in aerobic respiration, complex II catalyzes oxidation of succinate (succinate–ubiquinone reductase; SQR) in the mitochondria. The last step of the PEPCK-succinate pathway involves the NADH–fumarate reductase system, which is composed of complex I (NADH–quinone reductase), low-potential rhodoquinone (RQ) and complex II (QFR) [3,8]. Electron transfer from NADH to fumarate is coupled to ATP synthesis by site I phosphorylation in complex I. The difference in redox potential between NAD^+/NADH ($Em' = -320$ mV) and fumarate/succinate ($Em' = +30$ mV) is sufficient to drive ATP synthesis.

In eukaryotes, complex II is localized in the inner mitochondrial membrane, and is generally composed of 4 peptides [3]. The largest flavoprotein (Fp) subunit has an approximate molecular mass of 70 kDa and contains flavin adenine dinucleotide (FAD) as a prosthetic group. The relatively hydrophilic catalytic region of complex II is formed by the Fp subunit and the iron–sulfur cluster (Ip) subunit, whose molecular weight is about 30 kDa. The remaining subunits comprise cytochrome *b*, which contains heme *b*. Cytochrome *b* is composed of 2 hydrophobic membrane-anchoring polypeptide subunits; the 15-kDa large subunit (CybL) and the 13-kDa small subunit (CybS). These cytochrome *b* subunits are necessary for interaction between complex II and hydrophobic membrane-associated quinones such as ubiquinone (UQ) and RQ. However, it is unclear how heme *b* is involved in the electron transfer between complex II and quinones.

In a previous study, we showed that *A. suum* mitochondria express stage-specific isoforms of complex II [5,6,9]. While there is no difference in the isoforms of the Ip and CybL subunits of complex II between L3 larvae and adult *A. suum*, they have different isoforms of the complex II subunits Fp (larval, Fp^L; adult, Fp^A) and CybS (larval, $CybS^L$; adult, $CybS^A$). Quinone species in the mitochondria also change during the life cycle of *A. suum*. In adult mitochondria, the predominant quinone is the low-potential rhodoquinone (RQ; $Em' = -63$ mV); in larvae, the predominant quinone is ubiquinone (UQ; $Em' = +110$ mV) [10]. A combination of SQR and UQ, and that of QFR and a low-potential quinone, such as RQ or menaquinone (MK), is also observed in *E. coli* and other bacteria during metabolic adaptation to changes in oxygen supply [11]. UQ has a higher potential than RQ; therefore, RQ is better suited to transferring electrons to fumarate than is UQ. In L2 and L3 *A. suum* larvae, UQ preferentially donates electrons to the cytochrome chain in the mitochondria. Thus, UQ participates in aerobic metabolism in *A. suum* larvae, whereas RQ participates in anaerobic metabolism in adult *A. suum*.

After ingestion by the definitive host, the L3 larvae penetrate the intestinal wall and reach to the lung migrating through the tissues such as liver and heart. The L3 larvae passes from lung via the trachea to the small intestine where they molt to L4 and develop into sexually maturate adult worms in the small intestine [12]. Although studies have shown a clear difference in energy metabolism between larval and adult *A. suum* mitochondria, little is known about changes in the properties of mitochondria (including respiration) during migration of *A. suum* larvae in the host.

In the present study, we examined changes in subunit composition of *A. suum* larval complex II from lung stage L3 (LL3) larvae obtained from rabbits. Enzymatic analyses showed that properties of LL3 mitochondria differed from those of L3 and adult mitochondria. Protein chemical analysis revealed that the change in complex II begins with the anchor CybS subunit, and then occurs in the Fp subunit.

2. Materials and methods

2.1. Parasites

A. suum adult worms were procured from a slaughterhouse in Tokyo, Japan. Third stage infective (L3) larvae and lung stage L3 (LL3) larvae were obtained as previously described [5,13]. All animals used in this study were acclimatized to the experimental conditions for 2 weeks before the experiment. Animal experiments were conducted in accordance with the protocols approved by the Animal Care and Use Committee, National

Institute of Animal Health (Approval nos. 589,712). For the preparation of LL3 larvae, Japanese white rabbits were made to ingest infective *A. suum* eggs (approximately 1.5×10^5 eggs per rabbit), and infected lungs were removed from the rabbits 7 days after ingestion of the eggs. The lungs were cut into 2-cm cubes using a razor blade, and the cubes were put into nylon mesh bags (KA1000, Eiken Kizai, Tokyo, Japan) in 50-ml polypropylene conical tubes filled with phosphate-buffered saline (PBS) containing 100 μg/ml penicillin and 100 μg/ml streptomycin. Those tubes were then kept in a humidified incubator at 37 °C for 4 to 5 h. During that incubation, the larvae dropped out of the bags into the bottom of the tubes. The larvae were then washed several times with fresh PBS in a 37 °C water bath. Contaminating erythrocytes from the host rabbits were eliminated by hemolysis, which was induced by washing the pellet containing LL3 larvae with pre-warmed tap water at 37 °C. The body length of the LL3 larvae, obtained from infected rabbit on day 7 post-infection, were 1.2–1.3 mm. They were slightly smaller than LL3 larvae derived from infected swine at the same post-infectious stage (1.5 mm) [14].

2.2. Preparation of mitochondria from L3, LL3 and adult *A. suum*

Mitochondria from L3 and adult *A. suum* muscle were prepared using the method described by Amino et al. [5]. Because that method was not applicable to LL3 mitochondria, we established the following method to obtain active mitochondria from LL3; the entire procedure was performed on ice or at 4 °C. The LL3 larvae were gently suspended in an equal volume of ice-cold suspension buffer containing 210 mM mannitol, 10 mM sucrose, 1 mM disodium EDTA and 50 mM Tris–HCl (pH 7.5), supplemented with 10 mM sodium malonate [15]. The LL3 larvae in the suspension were cut using a scalpel (No. 10 blade, Feather, Osaka, Japan) on a 90 × 75 × 3-mm custom-made glass plate with a hollow (diameter, 22 mm; depth, 3 mm) in the middle. The cut larvae were then homogenized with a hand-powered glass–glass homogenizer for 15 min, and the homogenate was centrifuged at 500 × g for 1 min. The resulting supernatant was centrifuged at 10,000 × g for 10 min to obtain the mitochondrial pellet. The pellet was resuspended in the suspension buffer and stored at −80 °C until used. The protein concentration of the mitochondria was determined using the method of Lowry [16], using bovine serum albumin as the standard.

2.3. Enzyme assay

All assays were performed at 25 °C, using 50 mM potassium phosphate (pH 7.5) as the reaction buffer. The SQR [17], succinate dehydrogenase (SDH) [18], QFR [19] and NADH–fumarate reductase [8] activities of mitochondria were assayed as described. The NADH-decyl UQ (-dUQ) and NADH-decyl RQ (-dRQ) assays were performed using the same method as the NADH–fumarate reductase activity assay, except that 60 μM dUQ or dRQ was used as the electron acceptor, instead of sodium fumarate.

2.4. Quantitative analysis of quinone in LL3 mitochondria

Quinones were extracted from lyophilized LL3 mitochondria, and were analyzed by reverse-phase HPLC as described by Miyadera et al. [20]. The concentrations of quinones were determined spectrophotometrically using the following extinction coefficients: for UQ, $E_{1\%1\ cm}$ at 275 nm = 158; for RQ, $E_{1\%1\ cm}$ at 283 nm = 141 [10].

2.5. Western blotting

Complex II from L3, LL3 and adult mitochondria was analyzed by Western blotting using the method of Towbin et al. [21]. The mitochondrial proteins were separated by SDS-PAGE, using a 7.5% acrylamide gel for the Fp subunit, and using a 10/20% gradient acrylamide gel (Daiichi, Tokyo, Japan) for the Ip and CybS subunits. The proteins were then transferred to a nitrocellulose membrane at 4 °C and 80 V for 1 h. The membranes were incubated with the following antibodies in Tris-buffered saline containing 0.05% (w/v) Tween 20 (TBST) and 2% (w/v) skim milk: anti-Fp monoclonal, diluted 1:3000 [18]; anti-$CybS^A$ monoclonal, diluted 1:5000 [5]; $CybS^L$ peptide-based polyclonal, diluted 1:300 [5]; mixture of anti-Ip and anti-CybS polyclonal, diluted 1:2000 [5]. Each membrane was then incubated for 30 min with one of the following alkaline phosphatase-conjugated secondary antibodies: goat anti-mouse IgG (for Fp and $CybS^A$), or goat anti-rabbit IgG (for $CybS^L$, Ip and CybS). The proteins were detected using the alkaline phosphatase method. The amount of protein was normalized to the intensity of the Ip subunit at each stage, using NIH Image (a free image analyzing program for the Macintosh, developed by National Institutes of Health (NIH); www.rsb.info.nih.gov/nih-image/download.html).

2.6. Solubilization of mitochondria for blue native (BN-) PAGE

Mitochondria from L3, LL3 and adult *A. suum* (1.5 μmol/min in SDH activity) were incubated on ice for 1 h in 0.5% (w/v) sucrose monolaurate (SML) and Native PAGE™ sample buffer containing 50 mM Bis–Tris, 6 N HCl, 50 mM NaCl, 10% (w/v) glycerol and 0.001% (w/v) Ponceau S in 10 mM Tris–HCl (pH 7.5) (User manual, version A 2006; www.invitrogen.com/content/sfs/manuals/nativepage_man.pdf, Invitrogen, Carlsbad, CA, USA). They were then ultracentrifuged at 200,000 × g and 4 °C for 1 h, and the resulting supernatant was subjected to BN-PAGE, as described below.

2.7. BN-PAGE, CBB staining, in-gel SDH activity staining and Western blotting

The solubilized mitochondria were subjected to BN-PAGE [22] using Native PAGE Novex 4–16% Bis–Tris gels (Invitrogen). Electrophoresis was performed at 4 °C, at 150 V for 1 h, and then at 250 V, voltage constant. The cathode and anode buffers were prepared according to the user's manual of the Native PAGE Novex Bis–Tris gel system. Following the BN-PAGE, CBB staining was performed according to the user's

manual. The SDH activity of mitochondrial protein of L3, LL3 and adult *A. suum* was detected as described elsewhere [18,23]. After the BN-PAGE (first dimension), the gel cut by lane from the first-dimensional gel was equilibrated with SDS-PAGE buffer, and was then loaded onto the second-dimensional gel (7.5% acrylamide gel for Fp, and 10/20% gradient acrylamide gels (Daiichi) for Ip and CybS). The subsequent analysis by Western blotting was performed as described above.

3. Results

3.1. Enzymatic properties of LL3 complex II

Because only a small amount of LL3 larvae was obtained, and because LL3 larvae were more resistant to homogenization than L3 larvae and adult worms, we tried to establish a specific and reproducible protocol for the preparation of mitochondria from LL3 larvae. We found that cutting LL3 larvae with a scalpel was an effective method of recovering active mitochondria. Using the established protocol, we obtained approximately 0.5 mg of mitochondria from 1 infected rabbit. Fig. 2 shows the results of comparative analysis of enzyme activities, relative to NADH–fumarate reductase activity, in L3, LL3 and adult mitochondria.

The Fp and Ip subunits form the hydrophilic catalytic portion of complex II, and act as a succinate dehydrogenase (SDH), catalyzing the oxidation of succinate by the water-soluble electron acceptor phenazine methosulfate. The L3 and LL3 mitochondria had almost identical levels of SDH activity, whereas the SDH activity of adult mitochondria was 2.7 to 3.9 times higher than that of L3 and LL3 mitochondria (Fig. 2A). SQR catalyzes electron transfer from succinate to the physiological electron acceptor, ubiquinone. Similarly, SQR activity of adult mitochondria was 1.8 to 3.9 times higher than that of L3 and LL3 mitochondria (Fig. 2B). QFR catalyzes a reaction that is the reverse of the reaction catalyzed by SQR. The QFR activity of LL3 mitochondria was higher than that of L3 and adult mitochondria (Fig. 2C). The NADH–fumarate

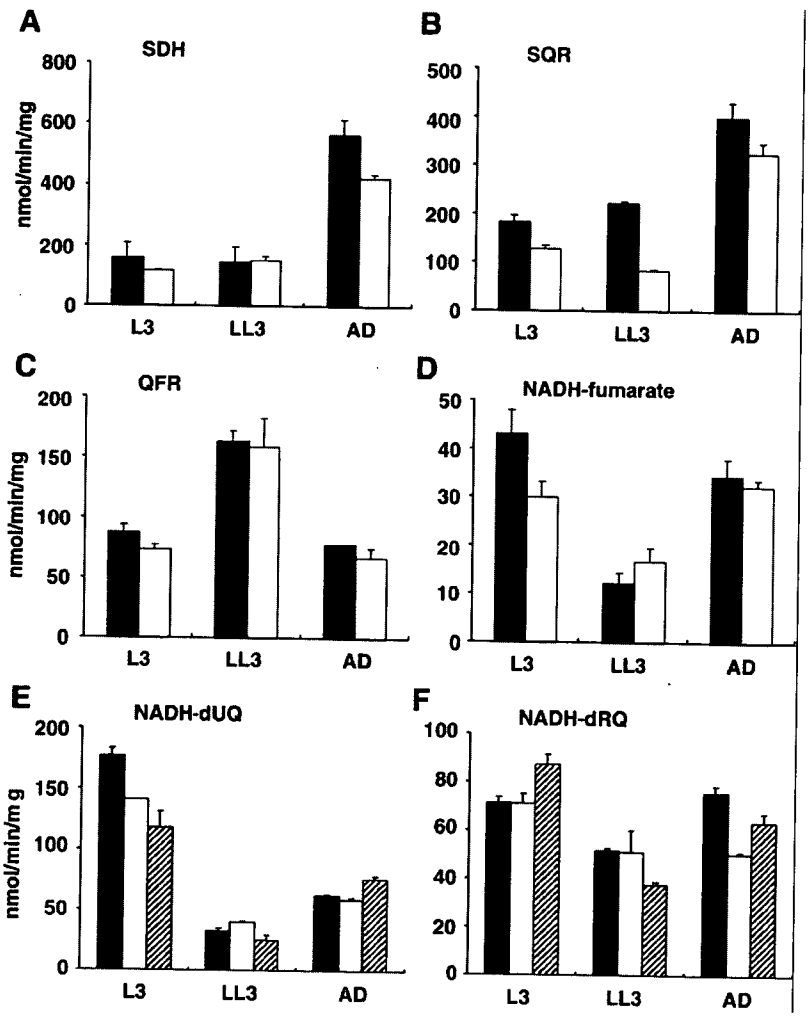

Fig. 2. Enzyme assay. Enzyme activities of complex I and II of mitochondria from L3 *A. suum* larvae, LL3 *A. suum* larvae, and *A. suum* adults. (A) SDH, (B) SQR, (C) QFR, (D) NADH–fumarate reductase, (E) NADH-dUQ and (F) NADH-dRQ. The mean and standard error were derived from triplicate measurements. Solid bars indicate experiment 1; open bars indicates experiment 2; stripe bars indicate experiment 3. Assays were performed as in materials and methods.

reductase system is an anaerobic electron-transport system of mitochondria, and is the terminal step of the PEPCK-succinate pathway. In the NADH–fumarate reductase system, the reducing equivalent of NADH is transferred to the low-potential RQ by the NADH-RQ reductase complex (Complex I). This pathway ends with the production of succinate by the rhodoquinol-fumarate reductase activity of complex II. Unexpectedly, the NADH–fumarate reductase activity of LL3 mitochondria was lower than that of L3 and adult mitochondria (Fig. 2D). The NADH-dUQ and NADH-dRQ activities of LL3 mitochondria were lower than those of L3 and adult mitochondria (Fig. 2E and F), suggesting that the low NADH–fumarate reductase activity of LL3 mitochondria is due to the lower activity of complex I in LL3 mitochondria.

3.2. Quinone components in LL3 mitochondria

Because quinone species are important low-molecular-weight mediators of electron transfer between respiratory enzymes, and because the ratio between RQ and UQ seems to be a critical factor in the direction of electron transfer in the chain, we examined the quinone content of LL3 mitochondria complex II. Although the amount of LL3 mitochondria that we obtained was quite limited, we performed the analysis using 2 different samples of LL3 mitochondria. The first sample of LL3 mitochondria contained 1.68 nmol/mg UQ-9 and 0.85 nmol/mg RQ-9. A similar result was obtained for the second sample (Table 1), indicating that the UQ content of LL3 mitochondria is approximately 2-fold greater than that of RQ. It should be noted that UQ-9 is the predominant quinone of L3 complex II (75% of the total quinone content), and that RQ is the only quinone present in complex II from adult *A. suum* muscle [10].

3.3. Subunit composition of the LL3 mitochondria complex II

To examine the subunit structure of complex II in LL3 mitochondria, we performed Western blotting. Because the isoforms of the Ip and CybL subunits do not change during the *A. suum* life cycle [5], the amount of proteins used for the Western blotting of Fp and CybS subunits was normalized to the intensity of the Ip subunit, which was visualized using the alkaline phosphatase method (Fig. 3D). LL3 mitochondrial complex II contained both Fp^L and Fp^A (Fig. 3). The LL3 and adult complex II had a Fp^L:Fp^A band intensity ratio of 1:0.56 and 1:3.5, respectively, whereas only the Fp^L band was observed in blots of L3 complex II (Fig. 3A). For the $CybS^A$ subunit, the

Table 1
Quinone quantitative analysis of LL3 mitochondria

Experiment	(nmol/mg) UQ-9[a]	RQ-9[b]	Ratio UQ-9[a]:RQ-9[b]
1	1.68	0.85	1.98:1
2	1.89	1.00	1.89:1

[a] UQ-9, ubiquinone-9.
[b] RQ-9, rhodoquinone-9.

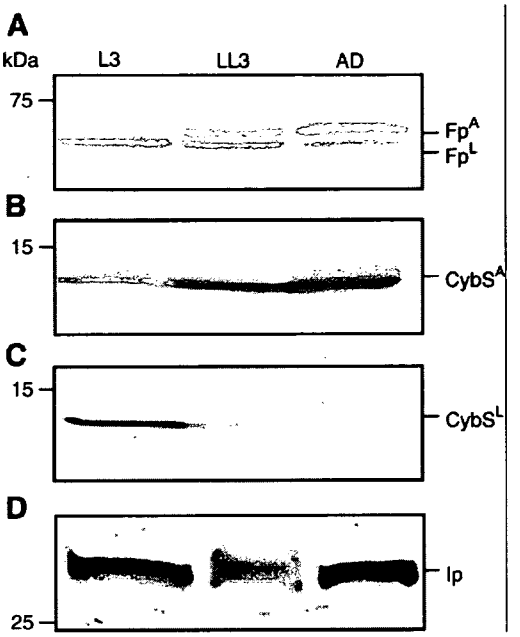

Fig. 3. Western blotting. Western blotting with (A) *A. suum* Fp monoclonal antibody, diluted 1:3000. (B) Monoclonal antibody against $CybS^A$ diluted 1:5000, and (C) Peptide-based polyclonal antibody against $CybS^L$ dituted 1:300. Protein levels were normalized to the Ip band intensity using (D) mixture of anti-Ip and anti-CybS polyclonal antibody diluted 1:2000. L3, *A. suum* larvae prepared from embryonated eggs; LL3, lung-stage L3; AD, *A. suum* adult. Precision Plus All Blue Standard (BIO-RAD).

L3:LL3:adult band intensity ratio was 1:3.5:6.1 (Fig. 3B). Only a small amount of $CybS^L$ was detected in LL3 mitochondria (<5% of $CybS^L$ in L3 mitochondria), and no $CybS^L$ was found in adult mitochondria (Fig. 3C). This result was reproducible in more than 3 experiments, suggesting that the subunit isoform change of LL3 complex II starts with CybS, and then occurs in Fp.

Because Western blotting clearly showed a difference in timing of isoform change between Fp and CybS subunits during migration in the host, we used BN-PAGE to examine the subunit composition of functional complex II. Mitochondrial proteins of each stage solubilized with sucrose monolaurate were subjected to BN-PAGE, and were then stained for CBB (Fig. 4A) or SDH activity (Fig. 4B) in the gel. Complex II from all 3 stages exhibited SDH activity in the gel, and band intensities of the 3 stages were almost identical when the amount of protein was normalized to 1.5 μmol/min SDH activity.

Next, we performed two-dimensional electrophoresis; with BN-PAGE as the first dimension, and SDS-PAGE as the second dimension. After the BN-PAGE, the gel was cut and was horizontally loaded onto SDS-PAGE. Following the two-dimensional electrophoresis, proteins were analyzed by Western blotting (Fig. 4C). Spots of Fps and CybSs were found in the same position as the SDH-stain band, indicating that native complex II with 4 subunits migrated during electrophoresis in the presence of the detergent. No extra spot was found in an area different from the SDH-stain position. In addition, the patterns

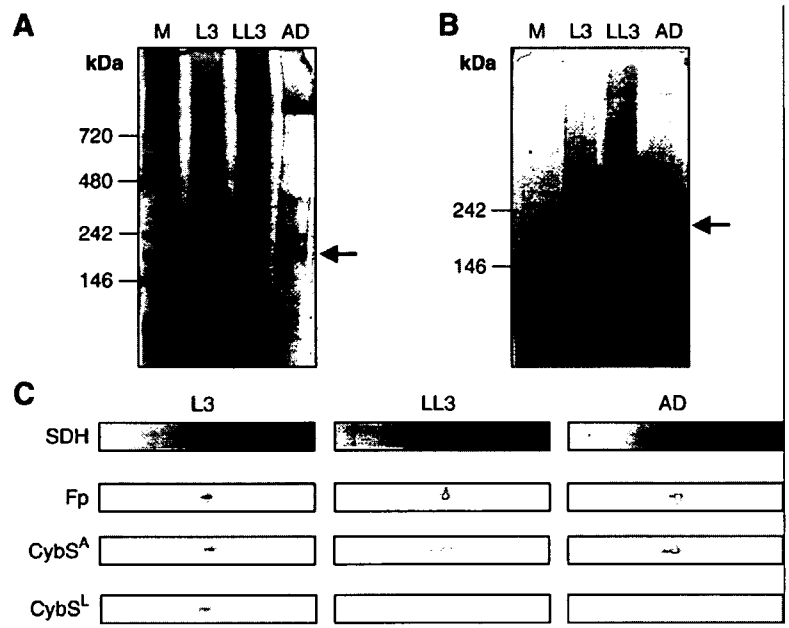

Fig. 4. BN-PAGE analysis. BN-PAGE analysis of mitochondria from *A. suum* L3 larvae, LL3 larvae and adults (1.5 μmol/min SDH activity). (A) CBB-stain. Arrow indicates expected SDH active bands. (B) SDH activity stained in gels of Native PAGE™ Bis–Tris gel (4–16%). Arrow shows SDH active bands. (C) Western blotting after SDS-PAGE, following BN-PAGE. Antibodies used were the same as in Fig. 3. The size marker is Native Mark Unstained Protein Standard (Invitrogen).

of intensity of the spots in Fig. 4C were almost identical to the results of Western blotting after SDS-PAGE (Fig. 3).

4. Discussion

In the present study, biochemical analyses of mitochondrial complex II were performed to elucidate how complex II in *A. suum* mitochondria change its isoform composition during migration in the mammalian host. In the first step of this study, we examined complex II from LL3 larvae (Fig. 1), because there is an established method of sample collection from rabbit lung, and because several properties of LL3 have been well studied [13,24]. The natural host of *A. suum* is swine so that we need pigs for developing the migratory phase and the adult stages. However, pig rearing facilities are currently quite limited for the purpose of doing *Ascaris* infection. Helminth researchers have previously examined the life cycle and worm burdens in rabbits [25,26]. The results showed that several criteria such as the organ migratory routes and recovery of larvae in rabbits were quite similar to those in pigs, indicating that rabbit can be fairly used for permissive hosts. Actually, *Ascaris* researchers including our group have employed rabbits to do biochemical experiments of the roundworms [27,28].

We previously demonstrated that *A. suum* mitochondria express stage-specific isoforms of complex II; i.e., the flavoprotein subunit (Fp) and the small subunit of cytochrome *b* (CybS) of complex II isolated from L3 infective eggs differ from those of adult muscle complex II, while the 2 forms of complex II have an identical iron-sulfur cluster subunit (Ip) and large subunit of cytochrome *b* (CybL). Therefore, the subunit isoform composition of complex II must change during migration in the host. To our surprise, Western blot analyses showed that both the Fp^L and Fp^A isoforms (in the ratio of 1: 0.56) were present in LL3 mitochondria, while the majority of CybS subunit was of the isoform $CybS^A$ (Fig. 3A and B). This means that expression of adult Fp does not synchronize with that expression of adult CybS, and suggests that LL3 complex II has a different combination of subunit isoforms than L3 and adult complex II.

To analyze the native state of complex II subunit composition in LL3 mitochondria, we used BN-/SDS-PAGE two-dimensional electrophoresis (Fig. 4C). The spots of the subunits were found at the same position as the SDH bands,

Table 2
Enzyme activities of L3, LL3 and adult complex I and II of *Ascaris suum* mitochondria

		Specific activity (nmol/min/mg)		
Assay	Experiment	L3	LL3	Adult
SDH	1	158±36	145±16	566±15
(complex II)	2	118±5.6	152±25	424±22
SQR	1	184±28	224±8.3	400±63
(complex II)	2	129±16	84.1±4.0	326±43
QFR	1	87.8±6.0	164±8.6	78.5±0.058
(complex II)	2	73.5±7.6	159±47	66.8±16
NADH–fumarate	1	43.0±10	12.3±4.4	34.4±7.1
reductase (complex I,II)	2	30.1±6.4	16.7±5.6	32.3±2.6
NADH-dUQ	1	177±12	32.3±5.6	62.4±1.9
	2	141±0.92	39.8±1.9	58.6±4.6
(complex I)	3	118±26	24.8±8.8	76.3±4.9
NADH-dRQ	1	71.4±4.4	51.6±2.0	75.7±5.6
	2	71.0±7.8	51.0±18	50.3±1.3
(complex I)	3	87.1±8.5	37.6±2.4	63.4±7.6

without any extra spots. This result indicates that the spots detected were derived from active complex II consisting of 4 subunits. In LL3 mitochondria, all 4 larva-/adult-types of Fp-CybS subunits was observed, while Fp^L, $CybS^A$ and $CybS^L$ subunit isoforms were detected in L3 mitochondria, and Fp^L, Fp^A and $CybS^A$ subunit isoforms were detected in adult mitochondria. The pattern of the intensity of the spots in Fig. 4C is consistent with that of the Western blotting after SDS-PAGE (Fig. 3), indicating that mitochondrial complex II subunit switching first occurs in CybS, and then occurs in Fp, during migration in the host.

Of the 4 possible Fp-CybS subunit combinations (Fp^L-$CybS^A$, Fp^A-$CybS^A$, Fp^L-$CybS^L$ and Fp^A-$CybS^L$), Fp^L-$CybS^A$ is the predominant combination in LL3 mitochondria. Western blot analysis of young adult mitochondria obtained from the muscle of 12-cm-long female worms showed that $CybS^L$ had completely disappeared, whereas Fp^L remained at a ratio of Fp^L:Fp^A = 1:1.5 (data not shown), although only 1 SDH band was observed in BN-PAGE. This finding may be due to similar properties between the 2 complexes with different combinations.

However, several questions remain unanswered. Because of limited sample amount, it is difficult to purify complex II from LL3 mitochondria. Reports indicate that adult *A. suum* uses the NADH–fumarate reductase system in its anaerobic host environment; in the NADH–fumarate reductase system, the QFR activity of mitochondrial complex II plays a significant role [3,29,30]. However, we previously found that L3 complex II had higher QFR activity than adult complex II, and presumed that this was due to pre-adaptation to the dramatic change in oxygen availability during infection of the host [5]. In the present study, we found that the QFR activity of LL3 complex II was twice as high as that of L3 complex II (Fig. 2C, Table 2). The host lung is a relatively aerobic environment (13.2% O_2) [31], suggesting that the larvae pre-adapt before they migrate into the anaerobic environment of the host small intestine (5% O_2).

Although LL3 mitochondria showed the highest QFR activity of the 3 stages we examined, their NADH–fumarate reductase activity was unexpectedly low (Fig. 2D). This appears to be due to the effects of low complex I activity, as indicated by the NADH-dUQ and NADH-dRQ assays (Fig. 2E and F). The NADH–fumarate reductase system is composed of complex I (initial dehydrogenase of NADH), RQ (electron mediator), and complex II (terminal oxidase for fumarate reduction). We also examined the quinone content of the mitochondria. Analysis of the quinone contents of mitochondria isolated from unembryonated eggs, L3 larvae and adult muscle showed that the predominant quinone in larval mitochondria (which possess an aerobic respiratory chain) was UQ-9 (75% of the total quinone content) [10]. In contrast, the only quinone present in anaerobic mitochondria from adult muscle is RQ-9. Consistent with these findings, reconstitution studies using bovine heart complex I and adult *A. suum* QFR show that RQ is essential for the function of the NADH–fumarate reductase system [32]. Specifically, when RQ-9 was incorporated into the system, the maximum activity of reconstituted NADH–fumarate reductase activity was 430 nmol/min/mg of *A. suum* complex II, while no activity was observed in the presence of UQ-9. In addition, our previous findings suggest that although *A. suum* adult complex I uses both RQ and UQ as electron acceptors, the 2 quinones have different ways of binding reaction and reaction with *A. suum* complex I [33]. It should be noted that in the present study, UQ accounted for 66% of the total quinone of LL3 complex II, which is an intermediate between those of L3 and adult complex II [10]. Further analysis of the effect of endogenous quinones in the mitochondria of the enzyme activities of complex I and complex II is needed to elucidate the unique properties of the NADH–fumarate reductase system of *A. suum*.

In the present study, we examined how mitochondrial complex II of *A. suum* changes its subunit composition, especially during migration in the host. We found that the small subunit of cytochrome *b* (CybS) starts to change its isoform before the flavoprotein (Fp) subunit does so. Further clarification of this process will require analysis of larvae from other migration stages in the host. In each stage, the metabolic pathway of *A. suum* may continue to change according to the environmental changes, even in the host body. To elucidate this dynamic change in the mitochondrial respiratory system of *A. suum* during migration, we plan to establish an experimental system using swine, which is a definitive host of *A. suum*. With such a system, further biochemical analysis should reveal novel properties of complex II in LL3 mitochondria.

Acknowledgements

We thank Dr. Tetsuro Ishii for his academic support. This study was supported by a grant-in-aid for scientific research on Priority Areas, for the 21st Century COE Program (F-3) and for Creative Scientific Research from the Japanese Ministry of Education, Science, Culture, Sports and Technology (180 73004, 18GS0314).

References

[1] Komuniecki R, Komuniecki PR. Aerobic–anaerobic transitions in energy metabolism during the development of the parasitic nematode *Ascaris suum*. In: Boothroyd JC, Komuniecki R, editors. Molecular approaches to parasitology. New York: Wiley-Liss; 1995.

[2] Tielens AGM, Rotte C, van Hellemond JJ, Martin W. Mitochondria as we don't know them. Trends Biochem Sci 2002;27:56–72.

[3] Kita K, Takamiya S. Electron-transfer complexes in *Ascaris* mitochondria. Adv Parasitol 2002;51:95–131.

[4] Kita K. Electron-transfer complexes in *Ascaris suum*. Parasitol Today 1992;8: 155–9.

[5] Amino H, Osanai A, Miyadera H, Shinjyo N, Tomitsuka E, Taka H, et al. Isolation and characterization of the stage-specific cytochrome *b* small subunit (CybS) of *Ascaris suum* complex II from the aerobic respiratory chain of larval mitochondria. Mol Biochem Parasitol 2003;128: 175–86.

[6] Amino H, Wang H, Hirawake H, Saruta F, Mizuchi D, Mineki R, et al. Stage-specific isoforms of *Ascaris suum* complex II: the fumarate reductase of the parasitic adult and the succinate dehydrogenase of free-living larvae share a common iron–sulfur subunit. Mol Biochem Parasitol 2000;106: 63–76.

[7] Kita K, Hirawake H, Miyadera H, Amino H, Takeo S. Role of complex II in anaerobic respiration of the parasite mitochondria from *Ascaris suum* and *Plasmodium falciparm*. Biochim Biophys Acta 2002;1553: 123–39.

[8] Omura S, Miyadera H, Ui H, Shiomi K, Yamaguchi Y, Masuma R, et al. An anthelmintic compound, nafredin, shows selective inhibition of

complex I in helminth mitochondria. Proc Natl Acad Sci U S A 2001;98: 60–2.
[9] Saruta F, Kuramochi T, Nakamura K, Takamiya S, Yu Y, Aoki T, et al. Stage-specific isoforms of complex II (succinate–ubiquinone oxidoreductase) in mitochondria from the parasitic nematode, *Ascaris suum*. J Biol Chem 1995;270:928–32.
[10] Takamiya S, Kita K, Wang H, Weinstein PP, Hiraishi A, Oya H, et al. Developmental changes in the respiratory chain of *Ascaris* mitochondria. Biochim Biophys Acta 1993;1141:65–74.
[11] Cole ST, Condon C, Lemire BD, Weiner JH. Molecular biology, biochemistry and bioenergetics of fumarate reductase, a complex membrane-bound iron-sulfur flavoenzyme of *Escherichia coli*. Biochim Biophys Acta 1985;811: 381–403.
[12] Heinz M. Encyclopedic reference of parasitology. 2nd ed. Berlin: Springer; 2001.
[13] Islam MK, Miyoshi T, Yamada M, Alim MA, Huang X, Motobu M, et al. Effect of piperazine (diethylenediamine) on the moulying proteome express and pyrophosphate activity of *Ascaris suum* lung-stage larvae. Acta Trop 2006;99:208–17.
[14] Miyazaki I. Helminthic zoonoses. Tokyo: International Medical Foundation of Japan; 1991. p. 295–305.
[15] Takamiya S, Furushima R, Oya H. Electron transfer complexes of *Ascaris suum* muscle mitochondria I. Characterization of NADH-cytochrome *c* reductase (complex I–III), with special reference to cytochrome localization. Mol Biochem Parasitol 1984;13: 121–34.
[16] Lowry OH, Rosebrough NJ, Farr AL, Randall RJ. Protein measurement with the folin phenol reagent. J Biol Chem 1951;193:265–75.
[17] Miyadera H, Shiomi K, Ui H, Yamaguchi Y, Masuma R, Tomoda H, et al. Atopenins, potent and specific inhibitors of mitochondrial complex II (succinate–ubiquinone oxidoreductase). Proc Natl Acad Sci U S A 2003;100: 473–7.
[18] Tomitsuka E, Goto Y, Taniwaki M, Kita K. Direct evidence for expression of Type II flavoprotein subunit in human complex II (succinate–ubiquinone reductase). Biochem Biophys Res Commun 2003;311: 774–9.
[19] Kita K, Vibat CR, Meinhardt S, Guest JR, Gennis RB. One-step purification from *Escherichia coli* of complex II (succinate:ubiquinone oxidoreductase) associated with succinate-reducible cytochrome b_{556}. J Biol Chem 1989;264:2672–7.
[20] Miyadera H, Amino H, Hiraishi A, Taka H, Murayama K, Miyoshi H, et al. Altered quinone biosynthesis in the long-lived *clk-1* mutants of *Caenohabditis elegans*. J Biol Chem 2001;276:7713–6.
[21] Towbin H, Staehelin T, Gorton J. Electrophoretic transfer of proteins from polyacrylamide gels to nitrocellulose sheets: procedure and some applications. Proc Natl Acad Sci U S A 1979;76: 4350–4.
[22] Shägger H, Cramer WA, von Jagow G. Analysis of molecular mass and oligomeric states of protein complexes by blue native electrophoresis and isolation of membrane protein complexes by two-dimensional native electrophoresis. Anal Biochem 1994;217:220–30.
[23] Kho CW, Park SG, Lee DH, Cho S, Oh GT, Kang S, et al. Activity staining of glutathione peroxidase after two-dimensional gel electrophoresis. Mol Cell 2004;18:369–73.
[24] Geenen PL, Bresciani J, Boes J, Pedersen A, Eriksen L, Fagerholm HP, et al. The morphogenesis of *Ascaris suum* to the infective third-stage larvae within the egg. J Parasitol 1999;85:616–22.
[25] Jeska EL, Williams JF, Cox DF. *Ascaris suum*: larval returns in rabbits, Guinea pigs and mice after low-dose exposure to eggs. Exp Parasitol 1969;26: 187–92.
[26] Stormberg BE, Soulsby EJL. *Ascaris suum*: immunization with soluble antigens in the Guinea pig. Int J Parasitol 1977;7:287–91.
[27] Komuniecki PR, Vanover L. Biochemical changes during the aerobic–anaerobic transition in *Ascaris suum* larvae. Mol Biochem Parasitol 1987;22(2–3):241–8.
[28] Islam MK, Miyoshi T, Kasuga-Aoki H, Isobe T, Arakawa Y, Matsumoto Y, et al. Inorganic pyrophosphatase in the roundworm *Ascaris* and its role in the development and molting process of the larval stage parasites. Eur J Biochem 2003;270: 2814–26.
[29] Kita K, Shiomi K, Omura S. Advances in drug discovery and biochemical studies. Trends Parasitol 2007;23:223–9.
[30] Kuramochi T, Hirawake H, Kojima S, Takamiya S, Furushima R, Aoki T, et al. Sequence comparison between the flavoprotein subunit of the fumarate reductase (complex II) of the anaerobic parasitic nematode, *Ascaris suum* and the succinate dehydrogenase of the aerobic, free-living nematode, *Caenorhabditis elegans*. Mol Biochem Parasitol 1994;68: 177–87.
[31] Martini FH, Ober WC, Garrison CW, Welch K, Hutching RT. Fundamentals of anatomy and physiology. 4th ed. Upper Saddle River, New Jergy: Prentice Hall; 1998.
[32] Kita K, Takamiya S, Furushima R, Ma YC, Suzuki H, Ozawa T, et al. Electron-transfer complexes of *Ascaris suum* muscle mitochondria. III. Composition and fumarate reductase activity of complex II. Biochim Biophys Acta 1998;935: 130–40.
[33] Yamashita T, Ino T, Miyoshi H, Sakamoto K, Osanai A, Nakamaru-Ogiso E, et al. Rhodoquinone reaction site of mitochondrial complex I, in parasitic helminth, *Ascaris suum*. Biochim Biophys Acta 2004;1608: 97–103.

Oleic acid is indispensable for intraerythrocytic proliferation of *Plasmodium falciparum*

F. MI-ICHI[1]†, S. KANO[2] *and* T. MITAMURA[1]*§

[1] *Department of Molecular Protozoology, Research Institute for Microbial Diseases, Osaka University, 3-1 Yamadaoka, Suita, Osaka 565-0871, Japan*
[2] *Research Institute, International Medical Center of Japan, 1-21-1 Toyama, Shinjuku, Tokyo 162-8655, Japan*

(Received 21 February 2007; revised 3 April and 22 May 2007; accepted 22 May 2007; first published online 5 July 2007)

SUMMARY

Serum-derived fatty acids are essential for the intraerythrocytic proliferation of *Plasmodium falciparum* in humans. We previously reported that only limited combinations of fatty acids can support long-term parasite culture, and palmitic acid ($C_{16:0}$)/oleic acid ($C_{18:1,n-9}$), palmitic acid ($C_{16:0}$)/vaccenic acid ($C_{18:1,n-7}$), or stearic acid ($C_{18:0}$) are required in these combinations, implying that these fatty acids are key molecules for intraerythrocytic parasite growth (Mi-Ichi *et al.* 2006). Here, we analysed profiles of parasitaemia changes as well as morphologies during the erythrocytic cycle and confirmed the importance of $C_{16:0}$ and $C_{18:1,n-9}$. We also provide evidence that $C_{18:1,n-9}$ but not other C18 monoenoic or dienoic acids maintain the synchronicity of parasite development in serum-free medium when paired with $C_{16:0}$, resulting in maintained exponential growth. Thus, $C_{18:1,n-9}$ is indispensable for the intraerythrocytic proliferation of *P. falciparum*.

Key words: malaria, lipid metabolism, fatty acid, cell cycle, apicomplexa.

INTRODUCTION

Plasmodium falciparum is the pathogen associated with the most severe form of malaria. Chloroquine, mefloquine and a variety of other drugs have been used for therapeutics and prophylaxis against *P. falciparum* but strains resistant to all of these antimalarials appeared in most regions where the disease is endemic. The clinical symptoms and pathogenesis of *P. falciparum*-induced malaria are associated exclusively with the asexual multiplication of this parasite during the erythrocytic cycle. We are interested in the intraerythrocytic proliferation of this parasite and in factors essential for growth.

Human serum-derived fatty acids are believed to be essential for the intraerythrocytic proliferation of *P. falciparum* (Holz, 1977; Vial and Ancelin, 1998). These fatty acids are metabolized to various lipid species, such as phosphatidylcholine, phosphatidylethanolamine, diacylglycerol and triacylglycerol, all of which are major constituents of membranes and lipid bodies in this parasite (Vial *et al.* 1982; Palacpac *et al.* 2004; Mi-Ichi *et al.* 2006). Although *P. falciparum* possesses the capacity for *de novo* fatty acid synthesis, most likely occurring in the apicoplast (Surolia and Surolia, 2001), the amount and kind of fatty acids produced by this pathway appear to be limited, and the major source of fatty acids is human serum (Mitamura *et al.* 2000; Mi-Ichi *et al.* 2006).

We recently reported that only limited combinations of human serum-derived fatty acids can support long-term parasite culture, and palmitic acid ($C_{16:0}$)/oleic acid ($C_{18:1,n-9}$), palmitic acid ($C_{16:0}$)/vaccenic acid ($C_{18:1,n-7}$), or stearic acid ($C_{18:0}$) are required in these combinations, implying that these fatty acids are key molecules for parasite growth (Mi-Ichi *et al.* 2006). These results led us to speculate that parasites show selectivity for the uptake and metabolism of serum-derived fatty acids. However, parasites are able to metabolize a broad range of fatty acids that are available in the environment (Mi-Ichi *et al.* 2006). This implies that *P. falciparum* may rely on fatty acid elongation and/or desaturation pathways for the synthesis of fatty acids that are essential for growth but are not available in the environment. Nevertheless, *P. falciparum* has been shown to utilize available fatty acids with limited modification (Mi-Ichi *et al.* 2006). These observations emphasize not only the uniqueness of fatty acid metabolism in *P. falciparum* but also the importance of key fatty acids for its intraerythrocytic proliferation. In this study, we analysed the roles of these fatty acids in the intraerythrocytic development of *P. falciparum* by

* Corresponding author: Research Institute, International Medical Center of Japan, 1-21-1 Toyama, Shinjuku, Tokyo 162-8655, Japan. Tel: +81-3-3202-7181 ext. 2871. Fax: +81-3-3202-7364. E-mail: tmitamura@ri.imcj.go.jp
† Present address: Department of Parasitology, Gunma University Graduate School of Medicine, 3-39-22 Showa-machi, Maebashi, Gunma 371-8511, Japan.
§ Present address: Research Institute, International Medical Center of Japan, 1-21-1 Toyama, Shinjuku, Tokyo 162-8655, Japan.

Parasitology (2007), **134**, 1671–1677.
doi:10.1017/S0031182007003137 Printed in the United Kingdom

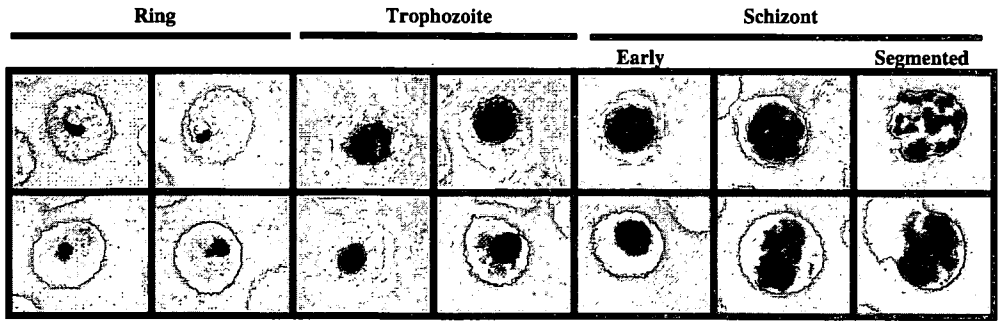

Fig. 1. Morphologies for normal appearance and abnormal appearance. The morphologies seen in the major populations at each stage are shown. The upper and lower rows indicate normal and abnormal appearances, respectively.

assessing their effects on morphology and parasite number.

MATERIALS AND METHODS

Materials

Fatty acids (>99%) and fatty acid-free bovine serum albumin (BSA) (catalogue no.A7511), used as lipid-free BSA (Mitamura *et al.* 2000), were purchased from Sigma-Aldrich (St Louis, MO). Concentrations of 600 μM reconstituted lipid-rich BSA containing 300 μM each of various fatty acids was prepared essentially as described previously (Mitamura *et al.* 2000). Basal medium, standard medium and serum-free medium supplemented with 60 μM lipid-rich BSA were as described previously (Palacpac *et al.* 2004).

Parasite culture

Cultures of the *P. falciparum* Honduras-1 isolate (Bhasin and Trager, 1984) were maintained routinely and synchronized occasionally as described previously (Hanada *et al.* 2000; Mitamura *et al.* 2000; Mi-Ichi *et al.* 2006). Aliquots of tightly synchronized parasite culture in serum-free medium supplemented with reconstituted lipid-rich BSA containing different fatty acids (5 ml culture with 3% haematocrit) were acquired at the indicated times and used for Giemsa-stained thin smears. Parasites of normal or abnormal appearance located within erythrocytes were counted separately. Normal or abnormal appearance was defined by parasite shape. Parasites with normal appearance clearly showed nuclei, brownish-yellow colored areas with black dots (assumed to be haemozoin within food vacuoles) and white dots (assumed to be lipid droplets), whereas parasites with abnormal appearance showed shrunken and dense, irregularly stained structures and did not show white dots (Fig. 1). Parasitaemia was determined by calculating the percentage of parasitized erythrocytes among at least 5000 erythrocytes and was an average of duplicate slides per sample. Counting of parasitized erythrocytes was performed by an investigator who was not notified of the experiment design. All experiments were performed twice. To monitor morphological changes, cells were imaged with an Olympus (Tokyo, Japan) BX50 microscope equipped with a Keyence (Osaka, Japan) high-sensitivity cooled CCD colour camera.

Statistics

Mantel-Haenszel Chi-Square statistics was used to assess the difference in stage distributions at the indicated time between medium containing $C_{16:0}$/$C_{18:1,n-9}$ and in that containing $C_{16:0}/C_{18:2,n-6}$ (Stokes *et al.* 1995). Kendall's τ-b statistics was used to evaluate the strength of association between the time and the distribution of stages during the course of intraerythrocytic development in each medium containing $C_{16:0}/C_{18:1,n-9}$ or $C_{16:0}/C_{18:2,n-6}$ (Stokes *et al.* 1995).

RESULTS AND DISCUSSION

As in standard medium (basal medium supplemented with 10% human serum), parasites grew well in serum-free medium supplemented with reconstituted lipid-rich BSA containing $C_{16:0}/C_{18:1,n-9}$; a 3-fold increase in parasitaemia was observed at 48 h (Fig. 2). However, in serum-free medium containing only either $C_{16:0}$ or $C_{18:1,n-9}$, parasitaemia of tightly synchronized cultures initiated with ring-stage parasites decreased dramatically during the course of the erythrocytic cycle. Parasitaemia was $\leqslant$0·2% at 48 h and nearly reached the low detection limit of microscopical quantification at 62 h in both media, regardless of the initial parasitaemias (0·65% or 1·57%) (Fig. 2).

Growth profiles in different media reflected changes in the number of erythrocytes infected by parasites with normal morphology (Fig. 1). However, parasites with abnormal appearance were also observed in all samples. Major morphologies observed in each sample at the indicated times are

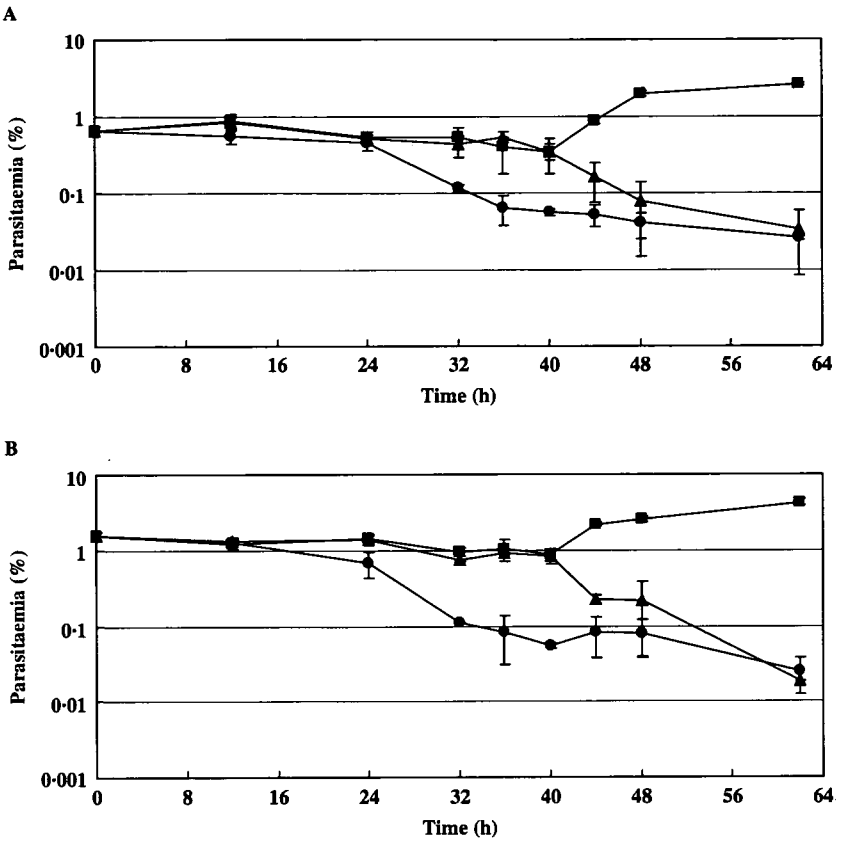

Fig. 2. Growth profiles of parasites in serum-free medium supplemented with reconstituted lipid-associated BSA containing a combination of fatty acids: $C_{16:0}$ (●); $C_{18:1,n-9}$ (▲); $C_{16:0}/C_{18:1,n-9}$ (■). Final concentrations of fatty acids used were $C_{16:0}$, 30 μM; $C_{18:1,n-9}$, 30 μM; $C_{16:0}/C_{18:1,n-9}$, 30 μM/30 μM. The tightly synchronized culture was set at ring with starting parasitaemia at 0·65% (A) and 1·57% (B). Error bar indicates the difference from the average.

shown in Fig. 3. In serum-free medium containing only $C_{16:0}$, rings did not develop into trophozoites but rather became pycnotic. In medium containing only $C_{18:1,n-9}$, rings developed into trophozoites and schizonts. Merozoites of shape similar to those in medium containing $C_{16:0}/C_{18:1,n-9}$ were observed at 40 h. However, apparently healthy rings (see Fig. 1) were not identified, even in cultures at 60 h (data not shown), implying that these merozoites were no longer released from the erythrocyte and gradually became pycnotic (48 and 52 h; data not shown). These results reflect the profiles of parasite growth in different media. Thus, it is likely that membranes necessary for development of healthy parasites are generated from saturated and unsaturated fatty acids. Alternatively, it may be that each fatty acid species exerts a distinct role on the intraerythrocytic development of *P. falciparum* because the time to arrest of intraerythrocytic development by $C_{16:0}$ differed from that by $C_{18:1,n-9}$. Detailed characterization of apparently normal trophozoites and schizonts and abnormal segmented schizonts in medium containing $C_{18:1,n-9}$ remains to be performed.

To examine the specificity of $C_{18:1,n-9}$ on the effect on intraerythrocytic development of *P. falciparum*, we compared $C_{18:1,n-9}$ with other unsaturated fatty acids of the same chain length but with different positions of the double bond or different degree of unsaturation ($C_{18:1,n-7}$ and $C_{18:2,n-6}$). We monitored parasitaemia for parasites of normal appearance in tightly synchronized cultures grown in serum-free medium supplemented with the lipid-rich BSA containing either $C_{18:1,n-7}$ or $C_{18:2,n-6}$ combined with $C_{16:0}$ (Fig. 4) because parasite growth does not occur in the presence of a single fatty acid (Mitamura *et al.* 2000; Fig. 2). In medium containing $C_{16:0}/C_{18:1,n-9}$, parasitaemia increased exponentially until 96 h (Fig. 4A). Cultures grown in medium containing $C_{16:0}/C_{18:1,n-7}$ showed a similar profile with exponential growth until 86 h. Beyond this time, however, parasitaemia plateaued and even decreased in long-term cultures at 138 h. In medium containing $C_{16:0}/C_{18:2,n-6}$, parasitaemia was decreased at 20 h. In addition, similar profiles were obtained regardless of the starting parasitaemia (0·13%, 0·65%, 1·6% or 3·5%) (Fig. 4B).

We next assessed populations of each stage in tightly synchronized cultures grown in serum-free medium containing $C_{16:0}/C_{18:1,n-9}$ or $C_{16:0}/C_{18:2,n-6}$ during the course of intraerythrocytic development,

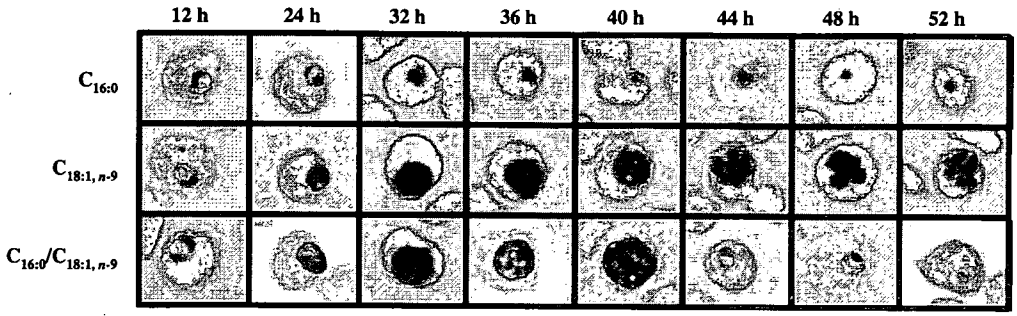

Fig. 3. Morphological changes over time of parasites grown in serum-free medium supplemented with reconstituted lipid-associated BSA containing a combination of fatty acids. Parasite morphology was observed under microscopy on Giemsa-stained slides. The fatty acids used are indicated at the left of each row. Final concentrations of fatty acids used were $C_{16:0}$, 30 μM; $C_{18:1,n-9}$, 30 μM; $C_{16:0}/C_{18:1,n-9}$, 30 μM/30 μM. Starting parasitaemia was set at 1·57%.

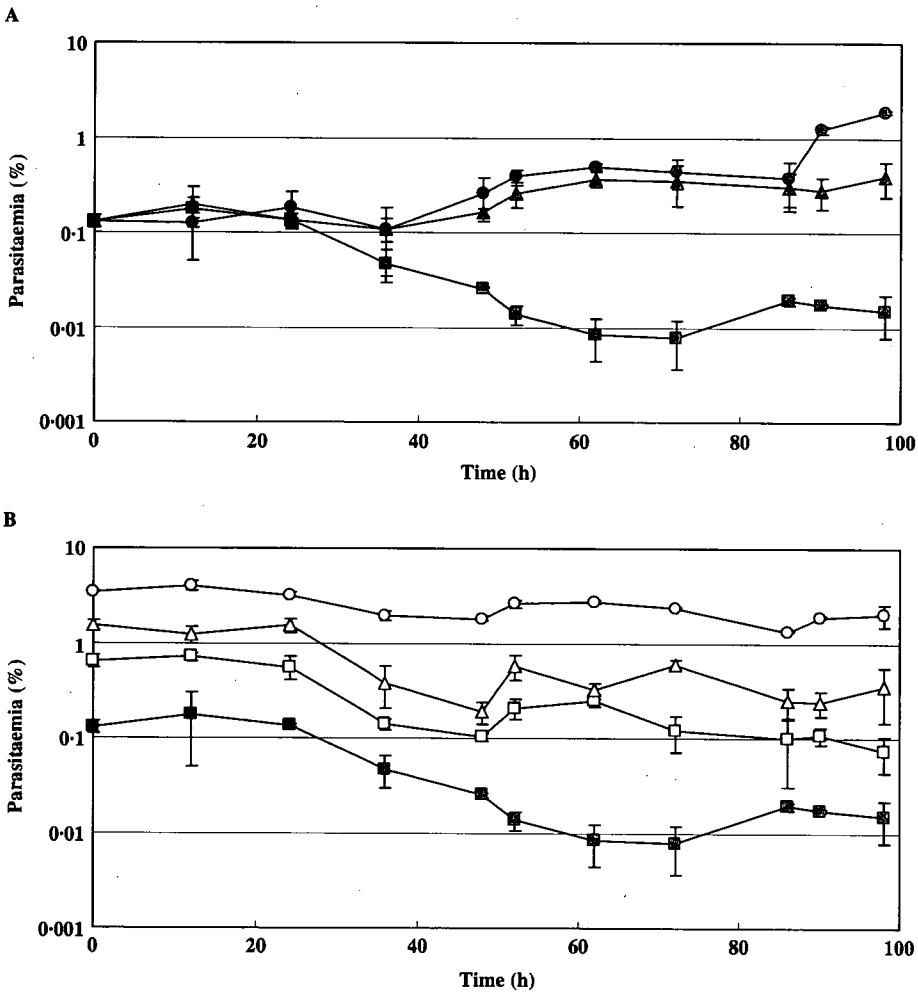

Fig. 4. Growth profiles of parasites in serum-free medium supplemented with reconstituted lipid-associated BSA containing a combination of fatty acids. (A) $C_{16:0}/C_{18:1,n-9}$ (●); $C_{16:0}/C_{18:1,n-7}$ (▲); $C_{16:0}/C_{18:2,n-6}$ (▩). Starting parasitaemia was set at 0·13%. (B) Growth profiles in serum-free medium containing $C_{16:0}/C_{18:2,n-6}$. Starting parasitaemia: 3·49% (○); 1·57% (Δ); 0·65% (□); 0·13% (■). Final concentrations of fatty acids used were $C_{16:0}/C_{18:1,n-9}$, 30 μM/30 μM; $C_{16:0}/C_{18:1,n-7}$, 30 μM/30 μM; $C_{16:0}/C_{18:2,n-6}$, 30 μM/30 μM. Error bar indicates the difference from the average.

noting whether parasites were of normal or abnormal morphology (Fig. 5). In medium containing $C_{16:0}/C_{18:1,n-9}$, parasites of normal appearance proceeded through stage progression and entered the next erythrocytic cycle by 40 h. Newly formed rings increased in number from 40 h to 52 h (Fig. 5A). In